THE JOURNAL OF PHYSICAL CHEMISTRY A

Article

pubs.acs.org/JPCA

Combined Experimental and Computational Study on the Unimolecular Decomposition of JP-8 Jet Fuel Surrogates. II: *n*-Dodecane (*n*-$C_{12}H_{26}$)

Long Zhao, Tao Yang, and Ralf I. Kaiser*

Department of Chemistry, University of Hawaii at Manoa, Honolulu, Hawaii 96822, United States

Tyler P. Troy and Musahid Ahmed*

Chemical Sciences Division, Lawrence Berkeley National Laboratory, Berkeley, California 94720, United States

Joao Marcelo Ribeiro, Daniel Belisario-Lara, and Alexander M. Mebel*

Department of Chemistry and Biochemistry, Florida International University, Miami, Florida 33199, United States

Supporting Information

ABSTRACT: We investigated temperature-dependent products in the pyrolysis of helium-seeded *n*-dodecane, which represents a surrogate of the *n*-alkane fraction of Jet Propellant-8 (JP-8) aviation fuel. The experiments were performed in a high temperature chemical reactor over a temperature range of 1200 K to 1600 K at a pressure of 600 Torr, with *in situ* identification of the nascent products in a supersonic molecular beam using single photon vacuum ultraviolet (VUV) photoionization coupled with the analysis of the ions in a reflectron time-of-flight mass spectrometer (ReTOF). For the first time, the initial decomposition products of *n*-dodecane—including radicals and thermally labile closed-shell species—were probed in experiments, which effectively exclude mass growth processes. A total of 15 different products were identified, such as molecular hydrogen (H_2), C2 to C7 1-alkenes [ethylene (C_2H_4) to 1-heptene (C_7H_{14})], C1−C3 radicals [methyl (CH_3), ethyl (C_2H_5), allyl (C_3H_5)], small C1−C3 hydrocarbons [acetylene (C_2H_2), allene (C_3H_4), methylacetylene (C_3H_4)], as well as the reaction products [1,3-butadiene (C_4H_6), 2-butene (C_4H_8)] attributed to higher-order processes. Electronic structure calculations carried out at the G3(CCSD,MP2)//B3LYP/6-311G(d,p) level of theory combined with RRKM/master equation of rate constants for relevant reaction steps showed that *n*-dodecane decomposes initially by a nonterminal C−C bond cleavage and producing a mixture of alkyl radicals from ethyl to decyl with approximately equal branching ratios. The alkyl radicals appear to be unstable under the experimental conditions and to rapidly dissociate either directly by C−C bond β-scission to produce ethylene (C_2H_4) plus a smaller 1-alkyl radical with the number of carbon atoms diminished by two or via 1,5-, 1,6-, or 1,7- 1,4-, 1,9-, or 1,8-H shifts followed by C−C β-scission producing alkenes from propene to 1-nonene together with smaller 1-alkyl radicals. The stability and hence the branching ratios of higher alkenes decrease as temperature increases. The C−C β-scission continues all the way to the propyl radical (C_3H_7), which dissociates to methyl (CH_3) plus ethylene (C_2H_4). In addition, at higher temperatures, another mechanism can contribute, in which hydrogen atoms abstract hydrogen from $C_{12}H_{26}$ producing various n-dodecyl radicals and these radicals then decompose by C−C bond β-scission to C3 to C11 alkenes.

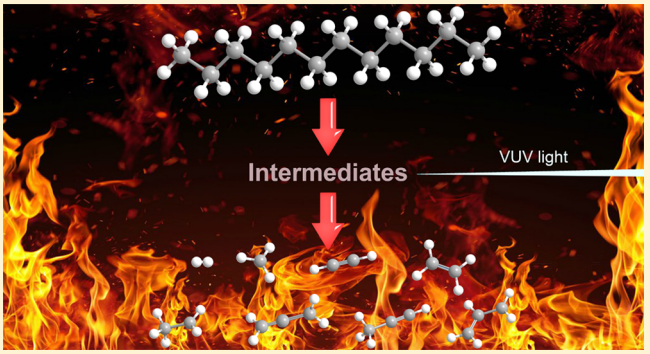

1. INTRODUCTION

Jet Propellant-8 (JP-8) represents a kerosene-based jet fuel which is widely used by the US military. It is comprised of hundreds of hydrocarbons which include aliphatic molecules (33−61% *n*-alkanes and isoalkanes; 1−5% olefins), monocyclic "paraffins" (10−20%), alkyl-substituted benzenes (12−22%), and polycyclic aromatic hydrocarbons (PAHs) (10−20%). Combustion scientists have been exploiting surrogate fuels in an attempt to convincingly model the performance along with emission characteristics of JP-8 engines.[1−24] While single-component surrogate fuels are suitable to replicate combustion efficiencies, multicomponent surrogates are essential to adequately model the chemistry of soot formation and flames.[25]

Received: November 23, 2016
Revised: January 6, 2017
Published: January 16, 2017

DOI: 10.1021/acs.jpca.6b11817
J. Phys. Chem. A 2017, 121, 1281−1297

Table 1. Compilation of Previous Experimental Studies on the Pyrolysis of *n*-Dodecane

group	method	temperature (K)	pressure (atm)	residence time (ms)	ref.
Brezinsky	high-pressure shock tube	867−1739	22.84, 49.42	1.15−3.47	30
Davidson	shock tube	990−1520	17−23	2	31
Banerjee	flow reactor	1000−1300	1	0−40	32
Bounaceur	flow reactor	950, 1000, and 1050	1	200	33
Herbinet	JSR	773−1073	1	1000−5000	34
Zhou	flow reactor	623−893	1	3300−12300	35
Eser	stainless steel tubing bomb reactor	673−723	10−100	9.0E8−3.6E9	36 and 37

These kinetic models require precise input parameters and an accurate knowledge of the initial steps, which initiate bond rupture in JP-8 surrogates. These processes essentially supply a pool of highly reactive radicals—often aromatic radicals (AR) and resonantly stabilized free radicals (RSFRs)—ultimately managing the autoignition and successive oxidation processes under combustion relevant conditions of temperatures of up to 1600 K and pressures up to a few atmospheres.[10,26−29] Previous experimental studies on the decomposition of the aliphatic component of JP-8 exploited *n*-dodecane ($C_{12}H_{26}$) as surrogates. These studies utilized high pressure shock tubes, flow reactors, jet stirred reactors, and micro reactors covering temperatures from 673 to 1739 K and pressures from 0.68 to 100 atm with diverging residence times of up to a few thousands of milliseconds (Table 1). In principle, these experiments revealed that the decomposition and "pyrolysis" of these surrogates lead to smaller C1 to C12 hydrocarbon molecules, but also reveal mass growth processed leading eventually to polycyclic aromatic hydrocarbons (PAHs) (Table S1).

The studies of *n*-dodecane thermal decomposition can be traced back to the 1980s. With high-pressure single pulse shock tube setups, Malewicki and Brezinsky[30] performed an experimental and modeling study on the pyrolysis and oxidation of *n*-dodecane. The experiment covered the temperature range from 867 to 1739 K, pressures from 19 to 74 atm, reaction times from 1.15 to 3.47 ms, and equivalence ratios from 0.46 to 2.05 and ∞. They measured the major hydrocarbon intermediates during *n*-dodecane pyrolysis experiments including ethylene (C_2H_4), methane (CH_4), propylene (C_3H_6), acetylene (C_2H_2), ethane (C_2H_6), 1-butene (C_4H_8), 1,3-butadiene (C_4H_6), 1-hexene (C_6H_{12}), 1-pentene (C_5H_{10}), 1-heptene (C_7H_{14}), 1-octene (C_8H_{16}), vinylacetylene (C_4H_4), 1-nonene (C_9H_{18}), and 1-decene ($C_{10}H_{20}$). Davidson et al.[31] utilized high-pressure shock tubes to detect the pyrolysis of three hydrocarbons including *n*-dodecane, methylcyclohexane, and *iso*-cetane from 990 to 1520 K at 17−23 atm. The fuel decomposition rates and ethylene yields were reported. They found that *iso*-cetane decomposes much faster than *n*-dodecane and MCH decomposes much slower than *n*-dodecane. n-Dodecane decomposition resulted in negligible amounts of propene and 1-butene at the conditions of 20 atm and 1000−1500 K. Later, Banerjee et al.[32] performed an experimental and modeling study on the pyrolysis and oxidation of *n*-dodecane exploiting a flow reaction in a temperature range of 1000−1300 K, a pressure of 1 atm, and a residence time up to 40 ms. They found that over the temperature of 1000 K, the process can be divided into two stages, decomposition of the fuel and its intermediates. The second step of intermediate decomposition is always rate limiting. Bounaceur et al.[33] presented experimental results for *n*-dodecane pyrolysis from 950 to 1050 K at 1 atm. The time-history of several hydrocarbon intermediates and final products were measured including methane (CH_4), ethane (C_2H_6), acetylene (C_2H_2), ethylene (C_2H_4), propene (C_3H_6), 1-butene (C_4H_8), 1,3-butadiene (C_4H_6), 1-pentene (C_5H_{10}), 1-hexene (C_6H_{12}) 1,3-hexadiene (C_6H_{10}), and 1-heptene (C_7H_{14}). By using a jet-stirred reactor, Herbinet et al.[34] carried out an experimental and kinetic modeling study on the thermal decomposition of *n*-dodecane in the temperature range from 773 to 1073 K at residence times between 1 and 5 s at atmospheric pressure. This study observed products including hydrogen (H_2), methane (CH_4), ethane (C_2H_6), 1,3-butadiene (C_4H_6), and 1-alkenes from ethylene (C_2H_4) to 1-undecene ($C_{11}H_{22}$). And at higher temperatures and residence times, mass growth processes to monocyclic and polycyclic aromatic species were observed. Zhou et al.[35] presented a flow reactor pyrolysis study on several higher molecular weight straight-chain alkanes including *n*-dodecane within a temperature range from 623 to 893 K at atmospheric pressure. The residence time ranged from 3.3 to 12.3 s. In this study, the authors found the 1-alkene selectivity strongly depends upon the system pressure in the pyrolysis of straight-chain alkanes as major products. The lower the pressure, the higher this selectivity. Yu and Eser[36,37] used a stainless steel tubing bomb reactor to study the near-critical and supercritical phase thermal decomposition of C10−C14 alkanes at 673−723 K and 1−10 MPa. They observed the relative yields of the primary (*n*-alkanes and 1-alkenes) and secondary products (*cis*- and *trans*-2-alkenes, smaller normal and branched alkanes) are dependent upon the reaction conditions (pressure/loading ratio, conversion, and temperature). As pressure increases, the yields of C6−Cm−1 *n*-alkanes and Cm+ alkanes (m is the number of carbon atoms in the reactant) increase and qthe yields of 1-alkenes and C1−C3 *n*-alkanes decrease. And high temperature favors the formation of 1-alkenes.

Besides the aforementioned experimental studies, kinetic modeling projects on *n*-dodecane pyrolysis were also carried in the recent years. With the MAMOX++ program, Ranzi et al.[38] generated a wide-range kinetic modeling study of the pyrolysis, partial oxidation and combustion of large *n*-alkanes, including *n*-decane, *n*-dodecane, and *n*-hexadecane. Later, they assembled the mechanisms for *n*-heptane and *n*-dodecane oxidation and reduced them, with the lumping approach proposed for the detailed mechanism.[39] Battin-Leclerc et al.[34,40] built up kinetic mechanisms of *n*-dodecane with EXGAS software to simulate several experimental data including JSR pyrolysis, JSR oxidation, shock tube ignition delay times, and turbulent flow reactor oxidation, for both high and low temperatures. In their studies, the NTC (negative temperature coefficient) region was reproduced for the JSR and shock tube experiments. Wang et al.[41] proposed a detailed kinetic model consisted of 1306 reactions and 171 species for the combustion of *n*-alkanes up to *n*-dodecane above 850 K, validated against several experimental data including flow reactor pyrolysis, JSR pyrolysis, laminar flame speeds and shock tube ignition delay times. In addition to their experimental study, Malewicki and Brezinsky[30] also performed a modeling study on the pyrolysis and oxidation of *n*-decane and

DOI: 10.1021/acs.jpca.6b11817
J. Phys. Chem. A 2017, 121, 1281−1297

n-dodecane. On the basis of their present and some previous literature data, they revised the kinetic model by Dooley et al.[42] Of particular interest, Westbrook and co-workers[43] carried out a comprehensive detailed chemical kinetic modeling for *n*-alkanes from *n*-octane to *n*-hexadecane. Their mechanism was designed to reproduce *n*-alkane oxidation at both low and high temperatures, and validated through extensive comparisons between computed and experimental data from a wide variety of different sources, including flow reactor pyrolysis, JSR pyrolysis, JSR oxidation, shock tube, and RCM ignition delay times. Recently, Narayanaswamy et al.[44] also presented a comprehensive kinetic modeling study for oxidation and pyrolysis of *n*-dodecane. They simulated several experimental data including ignition delay times, shock tube oxidation/pyrolysis speciation, flow reactor oxidation and burning velocity. The proposed reaction mechanism can describe the kinetics of *n*-dodecane, as well as that of *n*-heptane, *iso*-octane, and some substituted aromatics (toluene, styrene, ethylbenzene, *m*-xylene and 1-methylnaphthalene), which are important components of transportation fuel surrogates.

Very recently, we started a systematic research program to untangle the decomposition mechanisms of JP-8 surrogates by pyrolyzing helium-seeded *n*-decane (*n*-$C_{10}H_{22}$) in a chemical reactor at pressures of 600 Torr over a temperature range from 1100 to 1600 K.[45] The product distribution—including radicals and thermally labile closed-shell species—was probed on line and *in situ* in a supersonic molecular beam utilizing soft photoionization with single photon vacuum ultraviolet (VUV) photons followed by a mass spectroscopic analysis of the ions in a reflectron time-of-flight mass spectrometer (ReTOF), which can be utilized to identify and quantify products in the pyrolysis, especially radicals and isomers.[46−57] By limiting the residence time in the reactor to a couple of tens of microseconds, our major objectives are to explore the *initial* reaction *products* and aim to eliminate successive reactions of the initially formed species, which can lead to molecular mass growth processes. These studies reported multiple lower-mass C3−C7 hydrocarbons including alkenes, alkynes, and dienes along with C1 (methane) and C2 (acetylene, ethylene) as final products. Also, five radicals were observed in the *n*-decane pyrolysis including methyl, vinyl, ethyl, propargyl, and allyl. Further, the study presented branching ratios along with the underlying decomposition mechanisms. Here, we expand our studies to investigate via a combined theoretical and experimental strategy, the decomposition mechanisms of *n*-dodecane ($C_{12}H_{26}$) within the pyrolytic reactor and compare our findings with those data from previous high pressure shock tubes, flow reactors, and jet stirred reactor studies. It is our goal to provide both qualitative and quantitative identification of all nascent decomposition products (radicals and closed-shell molecules along with their structural isomers), the fundamental decomposition mechanisms, and reveal how their branching ratios depend on the temperature of the reactor. These data are of critical importance to the JP-8 modeling community to eventually optimize combustion efficiency and limit the production of toxic byproducts such as carcinogenic and mutagenic PAHs.

2. EXPERIMENTAL APPROACH

The experiments were conducted at the Advanced Light Source (ALS) at the Chemical Dynamics Beamline (9.0.2.) exploiting a "pyrolytic reactor". The experiment apparatus has been described before.[58−68] Briefly, the high temperature chemical reactor consists of a resistively heated silicon carbide (SiC) tube of 20 mm in length and 1 mm inner diameter. A gas mixture at a pressure of 600 Torr containing 0.0027% *n*-dodecane ($C_{12}H_{26}$) (Sigma-Aldrich; 99%+) in helium carrier gas (He; Airgas; 99.999%) is prepared by bubbling helium gas through *n*-dodecane stored in a stainless-steel bubbler held at 271 ± 1 K, the vapor pressure being 0.016 Torr at this temperature. The gas mixture was introduced into a resistively heated silicon carbide tube held at temperatures ranging from 1200 K to 1600 ± 5 K as monitored by a Type-C thermocouple in steps of 100 K. Here, photoionization efficiency (PIE) scan were performed with 0.05 eV intervals from 8.00 to 11.50 eV. For each temperature, the PIE scans were recorded three times and averaged; the experimental uncertainties were derived within 1σ as shown in the shaded areas in Figures 2−6. A set of additional mass spectra

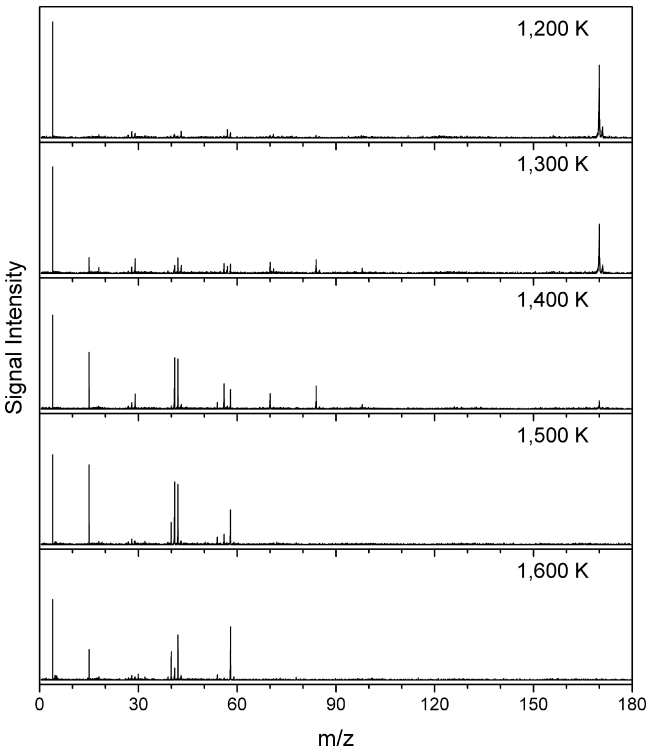

Figure 1. Mass spectra of the products obtained from the decomposition of *n*-dodecane recorded at a photon energy of 10.0 eV at different temperatures from 1200 to 1600 K.

was also taken at 15.5 eV to get extra information on hydrogen and methane (if they exist), which cannot be ionized at 11.5 eV. Pressures in the reactor at axial distances of 10 and 15 mm from the inlet are predicted to drop to about 60% and 30% of the inlet pressure based on simulations.[69] This would result in typically three to four (1600 K) collisions of a dodecane molecule with the helium atoms at these distances.

PIE analysis[46,47,55,57] and calculation of branching ratios were also performed to reveal trends in the formation of the products with increasing temperature. The detailed methods for PIE analysis and branching ratio calculation were also introduced in our previous work.[45] In brief, the PIE curves were fitted based on the known photoionization cross sections of corresponding species from the online database.[70] For the branching ratio calculation, for a certain species, since the ion count (normalized by the photon fluxes) presents a direct proportional relationship with the mole fraction (concentration), photoionization cross section and mass discrimination ($S_i(T, E) \propto X_i(T)\sigma_i(E)D_i$),[55]

DOI: 10.1021/acs.jpca.6b11817
J. Phys. Chem. A 2017, 121, 1281−1297

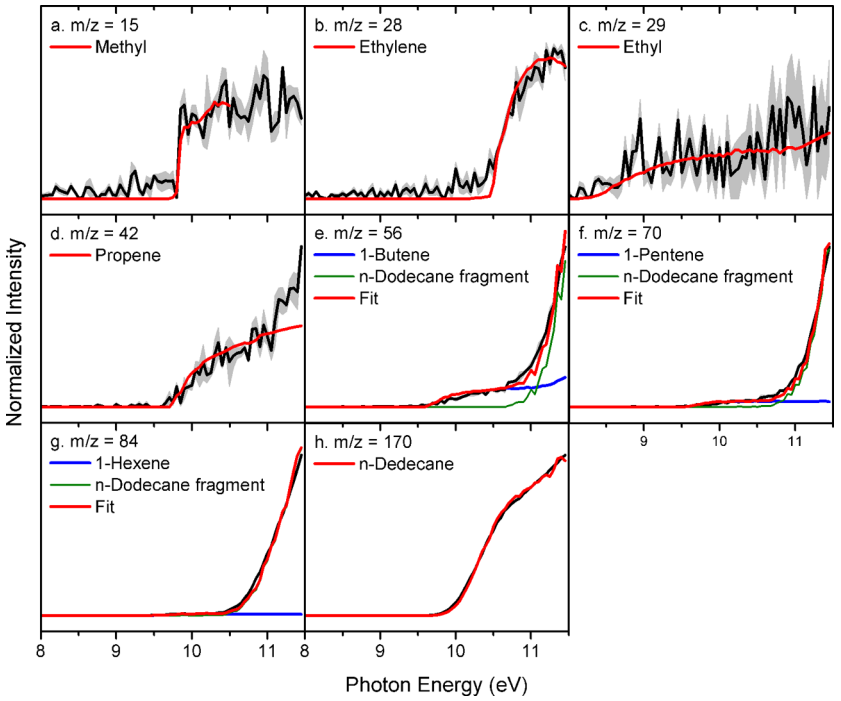

Figure 2. Experimental photoionization efficiency (PIE) curves (black lines) recorded from the decomposition of *n*-dodecane at 1200 K along with the experimental errors (gray area) and the reference PIE curves (red, green and blue lines).

and the ion counts were measured in the experiment, the cross sections can be looked up in the database, and then the relationship between the concentrations of individual products can be calculated ($\frac{X_i(T)}{X_j(T)} = \frac{S_i(T,E)}{S_j(T,E)} \cdot \frac{\sigma_j(E)}{\sigma_i(E)} \cdot \frac{D_j}{D_i}$). Subsequently the branching ratios can be worked out. Here, the branching ratios were computed by exploiting known photoionization cross sections at 9.5, 10.0, 10.5, 11.0, 11.5, and 15.5 eV with data obtained at 15.5 eV used to calculate the branching ratios of methane and hydrogen. The mass discrimination factors were taken from ref 68. The uncertainties of the photoionization cross sections of 15−20% were also taken into consideration.[56] In this work, the uncertainties of the cross section are chosen as 20%.

3. COMPUTATIONAL METHODS

Geometries of *n*-dodecane, its primary and secondary decomposition products, and transition states for secondary decomposition reactions (C−C bond β-scissions) and for direct H atom abstractions by hydrogen atoms have been optimized using the density functional B3LYP/6-311G(d,p) method. Vibrational frequencies of various stationary structures have been computed at the same level of theory. Then, relative energies for all optimized structures have been reevaluated by single-point calculations at the G3(CCSD,MP2) level of theory[71−73] with B3LYP/6-311G(d,p) zero-point vibrational energy corrections (ZPE), including the empirical higher level correction (HLC)[73] and using B3LYP/6-311G(d,p) optimized geometries. The inclusion of the HLC increases the calculated strengths of C−H bonds by 7 kJ/mol, decreases relative energies of transition states and products for the $C_{12}H_{26} + H \rightarrow C_{12}H_{25} + H_2$ hydrogen atom abstraction reactions also by 7 kJ/mol, is insignificant for C−C bond cleavages, and zero by definition for C−C bond β-scissions. The G3(CCSD,MP2)//B3LYP theoretical level has been shown to provide "chemical accuracy" within 3−6 kJ/mol in terms of average absolute deviations of relative energies of various stationary structures.[72] The ab initio calculations were performed using the GAUSSIAN 09[74] and MOLPRO 2010[75] program packages.

Rate constants for primary and secondary reactions involved in the pyrolysis of *n*-dodecane have been calculated using the RRKM/master equation approach[76] with the MESS package,[77] generally utilizing the rigid-rotor, harmonic-oscillator (RRHO) approximation for the evaluation of partition functions for molecular complexes and transition states. Collisional energy transfer rates in the master equation were expressed using the "exponential down" model,[78] with the temperature dependence of the range parameter α for the deactivating wing of the energy transfer function expressed as $\alpha(T) = \alpha_{300}(T/300\ \mathrm{K})^n$, with $n = 0.86$ and $\alpha_{300} = 228\ \mathrm{cm}^{-1}$ obtained earlier from classical trajectories calculations as "universal" parameters for hydrocarbons in the nitrogen bath gas.[79] We used the Lennard-Jones parameters (ε/cm^{-1}, σ/Å) = (253, 5.16) for the *n*-dodecane/nitrogen system derived by Jasper et al.[78] based on the fit of results using the "one-dimensional optimization" method.[80]

Since our goal in this work is both qualitative and quantitative evaluation of relative yields of various products at different stages of the pyrolysis in order to account for the observed experimental results, we used a simplified approximation to treat C−C and C−H single bond cleavages in the original *n*-dodecane molecule occurring without barriers. In particular, rate constants for these reactions were calculated using phase space theory with empirical potential energy parameters selected in such a way that the rate constants for the reverse $C_xH_y + C_{12-x}H_{26-y}$ and $C_{12}H_{25} + H$ radical recombination reactions reproduce the rate constants for the prototype $CH_3 + CH_3$ and $C_2H_5 + H$ reactions in the experimental 1200−1600 K temperature interval studied earlier by Klippenstein and co-workers[81,82] using the most accurate up-to-date theoretical approach, variable reaction coordinated transition state theory (VRC-TST). Another theoretical issue is the appropriate treatment of soft normal modes in $C_{12}H_{26}$ and $C_{12}H_{25}$ radicals, which are represented by convoluted coupled hindered rotations. Identification of such hindered rotors and

DOI: 10.1021/acs.jpca.6b11817
J. Phys. Chem. A 2017, 121, 1281−1297

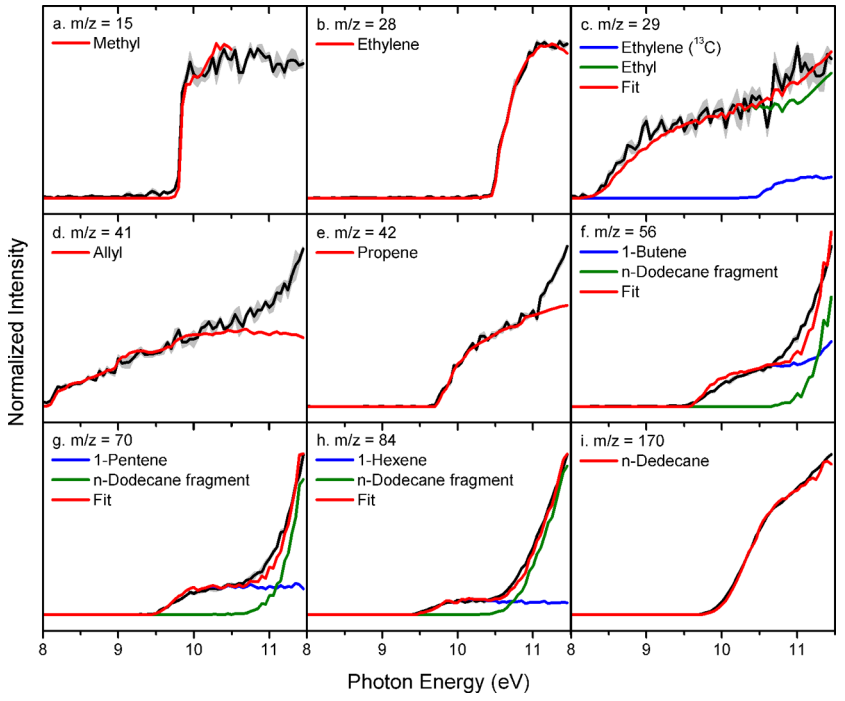

Figure 3. Experimental photoionization efficiency (PIE) curves (black lines) recorded from the decomposition of *n*-dodecane at 1300 K along with the experimental errors (gray area) and the reference PIE curves (red, green, and blue lines). For m/z = 41 and 42, there may be some photoionization fragments from initial decomposition products causing the experimental values to be higher than the fittings at higher energies.

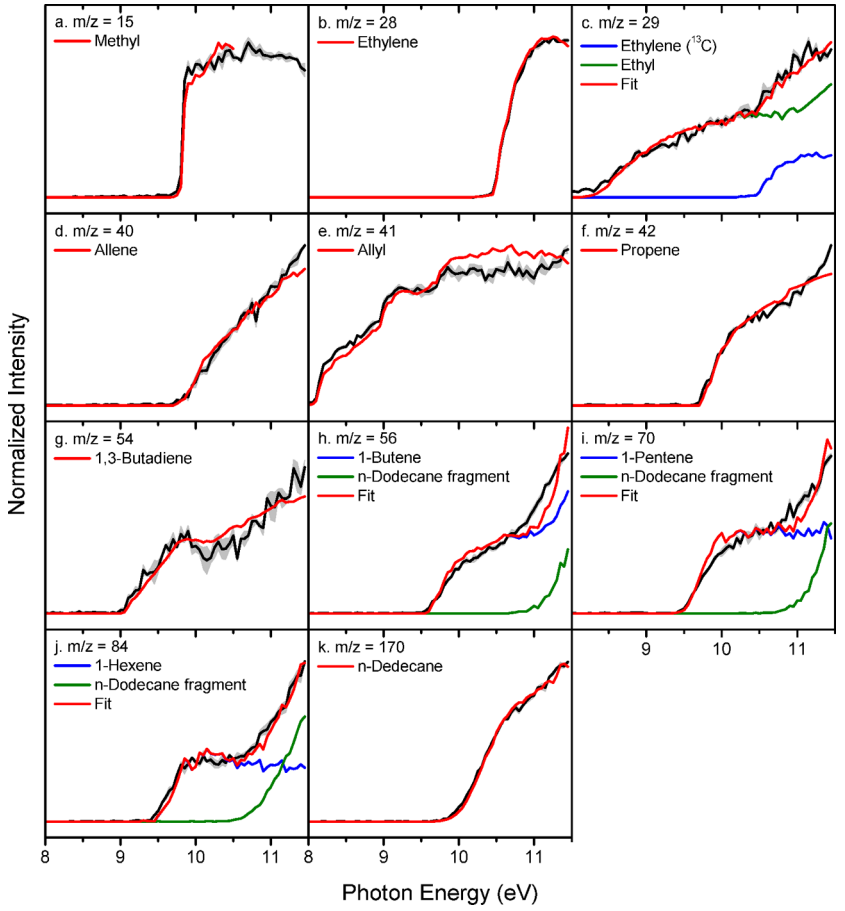

Figure 4. Experimental photoionization efficiency (PIE) curves (black lines) recorded from the decomposition of *n*-dodecane at 1400 K along with the experimental errors (gray area) and the reference PIE curves (red, green, and blue lines).

DOI: 10.1021/acs.jpca.6b11817
J. Phys. Chem. A 2017, 121, 1281−1297

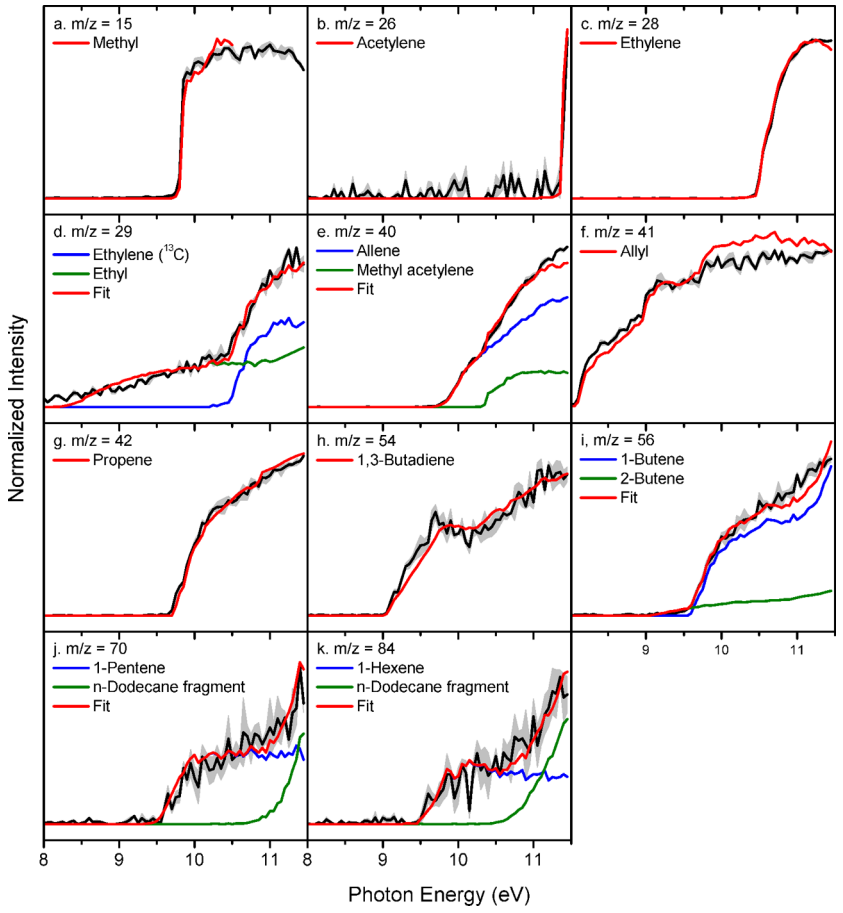

Figure 5. Experimental photoionization efficiency (PIE) curves (black lines) recorded from the decomposition of *n*-dodecane at 1500 K along with the experimental errors (gray area) and the reference PIE curves (red, green, and blue lines).

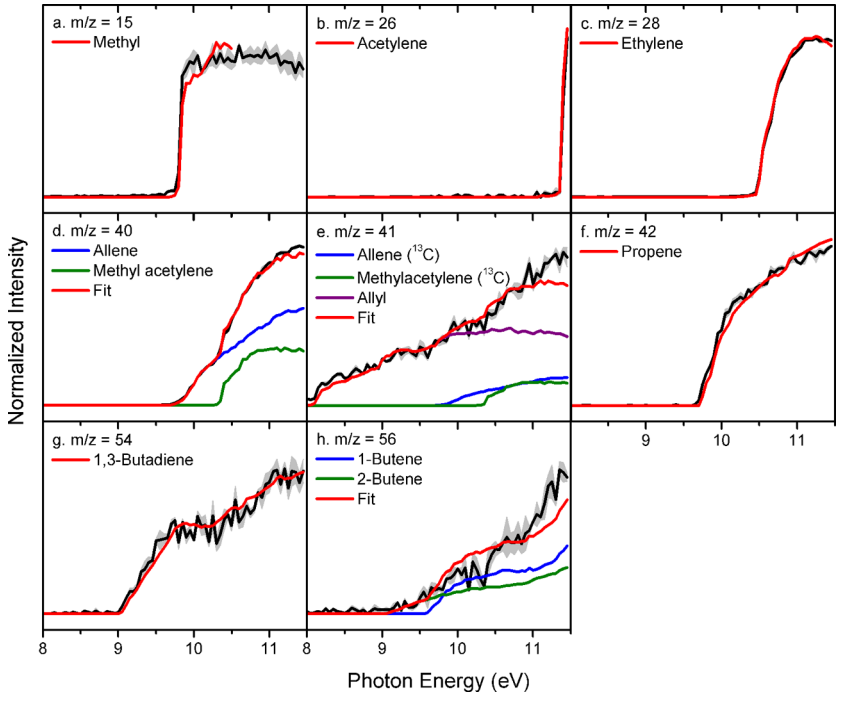

Figure 6. Experimental photoionization efficiency (PIE) curves (black lines) recorded from the decomposition of *n*-dodecane at 1600 K along with the experimental errors (gray area) and the reference PIE curves (red, green, blue and purple lines).

evaluation of their potential energy profiles in long alkanes is an extremely complex task. However, in our previous work, we showed that in smaller 1-alkyl radicals, from C_3H_7 to C_9H_{19}, the replacement of harmonic oscillators with hindered rotors

DOI: 10.1021/acs.jpca.6b11817
J. Phys. Chem. A 2017, 121, 1281−1297

Table 2. Compilation of Products Observed in the Present Experiments on the Decomposition of *n*-Dodecane[a]

Molecule	Formula	Mass	Structure
Hydrogen	H_2	2	H—H
Methyl radical	CH_3	15	CH_3•
Acetylene	C_2H_2	26	
Ethylene	C_2H_4	28	
Ethyl radical	C_2H_5	29	
Allene	C_3H_4	40	C
Methylacetylene	C_3H_4	40	
Allyl radical	C_3H_5	41	
Propene	C_3H_6	42	
1,3-Butadiene	C_4H_6	54	
1-Butene	C_4H_8	56	
2-Butene	C_4H_8	56	
1-Pentene	C_5H_{10}	70	
1-Hexene	C_6H_{12}	84	
1-Heptene	C_7H_{14}	98	

[a]The species highlighted in bold were detected for the first time in *n*-dodecane pyrolysis.

Table 3. Branching Fractions of the Products in the Decomposition of *n*-Dodecane at 600 Torr in the Chemical Reactor at 1200, 1300, 1400, 1500, and 1600 K

			temperature				
species[a]	formula	mass	1200 K	1300 K	1400 K	1500 K	1600 K
hydrogen	H_2	2	–	6.63 ± 1.99	3.68 ± 0.97	4.95 ± 1.15	11.40 ± 3.22
methyl radical	CH_3	15	10.41 ± 3.60	9.38 ± 2.32	11.63 ± 2.53	13.15 ± 2.87	9.01 ± 2.41
acetylene	C_2H_2	26	–	–	–	0.23 ± 0.06	1.59 ± 0.36
ethylene	C_2H_4	28	29.85 ± 7.99	40.44 ± 8.71	52.35 ± 11.82	57.67 ± 13.03	60.28 ± 13.50
ethyl radical	C_2H_5	29	20.46 ± 6.32	8.68 ± 2.20	3.35 ± 0.80	0.85 ± 0.28	–
allene	C_3H_4	40	–	–	0.55 ± 0.18	2.74 ± 0.67	5.37 ± 1.16
methylacetylene	C_3H_4	40	–	–	–	0.52 ± 0.34	1.32 ± 0.86
allyl radical	C_3H_5	41	–	4.46 ± 1.29	8.02 ± 1.98	8.52 ± 2.16	1.79 ± 0.52
propene	C_3H_6	42	13.14 ± 4.19	10.70 ± 3.09	10.51 ± 2.59	8.85 ± 1.96	8.03 ± 1.80
1,3-butadiene	C_4H_6	54	–	–	0.34 ± 0.08	0.42 ± 0.09	0.38 ± 0.09
1-butene	C_4H_8	56	18.45 ± 6.50	12.49 ± 4.22	6.17 ± 1.84	1.59 ± 0.41	0.41 ± 0.14
2-butene	C_4H_8	56	–	–	–	0.08 ± 0.04	0.06 ± 0.03
1-pentene	C_5H_{10}	70	3.95 ± 1.56	3.01 ± 0.83	1.53 ± 0.40	0.18 ± 0.05	–
1-hexene	C_6H_{12}	84	3.74 ± 1.22	3.63 ± 0.83	1.67 ± 0.40	0.09 ± 0.03	–
1-heptene	C_7H_{14}	98	0.15 ± 0.07	1.00 ± 0.16	0.71 ± 0.09	–	–

[a]Note: As there is no cross section database of 1-heptene, its branching fraction cannot be calculated. Therefore, the normalized ion count intensities of 1-heptene at 10.0 eV are listed in the last row to reveal the trend of 1-heptene formation from 1200 to 1600 K.

increased the computed C−C β-scission rate constants by 8−41% at 1000 K and by only 2−25% at 1600 K.[45] Here, all calculations have been performed within RRHO keeping in mind the above-mentioned error bars in rate constants. The anticipated errors in ratios of rate constants are expected to be smaller than the errors in their absolute values due to cancelations of similar inaccuracies.

4. EXPERIMENTAL RESULTS

Figure 1 exhibits the mass spectra collected during the pyrolysis of *n*-dodecane ($C_{12}H_{26}$, m/z = 170) at an energy of 10.0 eV covering the temperature range from 1200 to 1600 K. The photon energy was chosen to be 10.0 eV to avoid the formation of fragment ions from dissociative photoionization of *n*-dodecane at photon energies higher than 10.5 eV. These fragments are labeled as "*n*-dodecane fragment" in Figures 2−6. The mass spectrometric data alone provide evidence of ion counts from m/z = 15 to m/z = 98 along with the parent ions of the ionized *n*-dodecane precursor at m/z = 170. No ion counts of molecules heavier than *n*-dodecane were observed at the experiment temperature. This requirement represents a crucial prerequisite for the extraction of the *initial* pyrolysis products of *n*-dodecane. The detected mass-to-charge ratios, as well as the chemical formulas and chemical structures of the products, are listed in Tables 2 and 3; species observed for the first time in a pyrolysis experiment of *n*-dodecane are emphasized in bold. The corresponding photoionization efficiency (PIE) curves along with the best fits are visualized in Figures 2−6 for all temperatures from 1200 to 1600 K. As outlined in the Experimental Approach, the individual PIE curves from m/z = 15 to m/z = 170 were fitted with the linear combination of known PIE curves of the corresponding species. Generally, the black lines in Figures 2−6 represent the experimental data of PIE curves in this work with the shaded area exhibiting the experimental uncertainties. The red lines are the overall best fit to the PIE curves. If the PIE curves have contributors of more than one species, the blue, green and purple lines are referred to the individual components. Literature PIE curves are taken from the

DOI: 10.1021/acs.jpca.6b11817
J. Phys. Chem. A 2017, 121, 1281−1297

Table 4. Photoionization Cross Sections (Mb) of the Species at Selected Energies Exploited for the Calculations of the Branching Ratios in This Work

			photon energy (eV)						
species	formula	mass	9.5	10.0	10.5	11.0	11.5	15.5	ref.
hydrogen	H_2	2	–	–	–	–	–	4.73	95
methyl radical	CH_3	15	–	4.78	5.81	–	–	–	96
acetylene	C_2H_2	26	–	–	–	–	18.258	–	57
ethylene	C_2H_4	28	–	–	0.918	7.794	8.016	–	97
ethyl radical	C_2H_5	29	4.36	5.05	5.52	5.64	5.37	–	98
allene	C_3H_4	40	–	5.66	15.48	22.26	25.84	–	99
methylacetylene	C_3H_4	40	–	–	23.06	43.84	42.1	–	97
allyl radical	C_3H_5	41	5.636	6.227	6.091	–	–	–	100
propene	C_3H_6	42	–	5.33	9.05	11.40	12.66	–	101
1,3-butadiene	C_4H_6	54	8.48	13.96	16.44	19.91	22.45	–	99
1-butene	C_4H_8	56	–	7.35	10.02	10.88	17.33	–	101
2-butene	C_4H_8	56	5.24	9.06	11.04	14.05	19.17	–	102
1-pentene	C_5H_{10}	70	0.62	14.38	14.90	14.83	13.92	–	102
1-hexene	C_6H_{12}	84	0.89	8.58	9.65	8.86	9.00	–	99
n-dodecane	$C_{12}H_{26}$	170	0.01	3.325	30.058	43.15	53.542	–	103

Table 5. Database and Measured Photoionization Energies of the Species in the PIE Scan

				photoionization energy (eV)				
species	formula	mass	database[70]	1200 K	1300 K	1400 K	1500 K	1600 K
methyl radical	CH_3	15	9.839	9.85	9.75	9.75	9.75	9.75
acetylene	C_2H_2	26	11.4	–	–	–	11.3	10.35
ethylene	C_2H_4	28	10.514	10.40	10.50	10.50	10.45	10.45
ethyl radical	C_2H_5	29	8.117	8.15	8.15	8.10	8.10	–
allene	C_3H_4	40	9.692	–	–	9.70	9.75	9.70
methylacetylene	C_3H_4	40	10.36	–	–	–	10.30	10.30
allyl radical	C_3H_5	41	8.18	–	8.10	8.10	8.10	8.10
propene	C_3H_6	42	9.73	9.75	9.70	9.75	9.70	9.70
1,3-butadiene	C_4H_6	54	9.072	–	–	9.05	9.05	9.05
1-butene	C_4H_8	56	9.55	9.55	9.55	9.55	9.60	9.55
2-butene	C_4H_8	56	9.11	–	–	–	9.10	9.15
1-pentene	C_5H_{10}	70	9.49	9.55	9.50	9.45	9.55	–
1-hexene	C_6H_{12}	84	9.44	9.45	9.45	9.45	9.45	–
1-heptene	C_7H_{14}	98	9.27	9.30	9.30	9.30	–	–
n-dodecane	$C_{12}H_{26}$	170	9.64[a]	9.65	9.65	9.65	–	–

[a]Note: based on the cross section curve of *n*-dodecane, the ionization energy is about 9.64 eV.

combustion chemistry database[70] and are individually referenced as well (Table 4). A detailed analysis of the temperature dependence of the PIE curves (Figures 2–6) as outlined above reveals interesting trends.

First, the intensity of the parent ion of *n*-dodecane (m/z = 170) decreases as the temperature drops from 60% (1200 K) via 48% (1300 K), 9% (1400 K), and eventually vanishes at 1500 K. This suggests that the decomposition of the *n*-dodecane precursor is complete at 1500 K.

Second, as compiled in Table 3, as the temperature increases, the number of pyrolysis products first rises from eight C1 to C7 species at 1200 K to ten (1300 K), twelve (1400 K), and fifteen products (1500 K) before ultimately decreasing to twelve C1-C4 products (1600 K). This trend proposes that as the temperature increases beyond 1400 K, degradation occurs for the initial higher molecular weight products from C4 to C6 hydrocarbons, especially for C5 and C6 transients, which are completely consumed at 1600 K.

Third, we have identified 15 products, which can be arranged into six groups. (i) a homologues series of alkenes [C2–C7; ethylene (C_2H_4), propene (C_3H_6), 1-butene (C_4H_8), 2-butene (C_4H_8), 1-pentene (C_5H_{10}), 1-hexene (C_6H_{12}), and 1-heptene (C_7H_{14})], (ii) diene [1,3-butadiene (C_4H_6)], (iii) cumulene [allene (C_3H_4)], (iv) alkynes [acetylene (C_2H_2), methylacetylene (C_3H_4)], (v) radicals [methyl (CH_3), ethyl (C_2H_5), allyl (C_3H_5)], and (vi) smaller products [hydrogen (H_2)]. The appearance energies (ionization onsets) of these products as determined in our experiments agree very well with the adiabatic ionization energies as compiled in Table 5 with deviations of less than 0.05 eV in cases of excellent signal-to-noise ratios of the PIE curves, but not more than 0.08 eV otherwise. Among these species, it is important to highlight that this technique is ideally suited to detect C1 to C3 radical species as pyrolysis products, among them the methyl (CH_3), ethyl (C_2H_5) and allyl (C_3H_5) radicals being detected for the first time in *n*-dodecane pyrolysis experiments. Compared with our previous *n*-decane investigation, methane, vinyl and propargyl were not observed in this *n*-dodecane pyrolysis. There might be two reasons: (1) the initial concentration of *n*-dodecane is lower by 88% compared with that of *n*-decane due to the lower vapor pressure;[45] (2) the branching ratios of these three species is much lower with respect to the other products.

Fourth, Table 3 and Figure 7 quantify that ethylene (C_2H_4) represents the major decomposition products of *n*-dodecane over the complete temperature range increasing from about 30% to 60% from 1200 to 1600 K. It is important to highlight that

DOI: 10.1021/acs.jpca.6b11817
J. Phys. Chem. A 2017, 121, 1281–1297

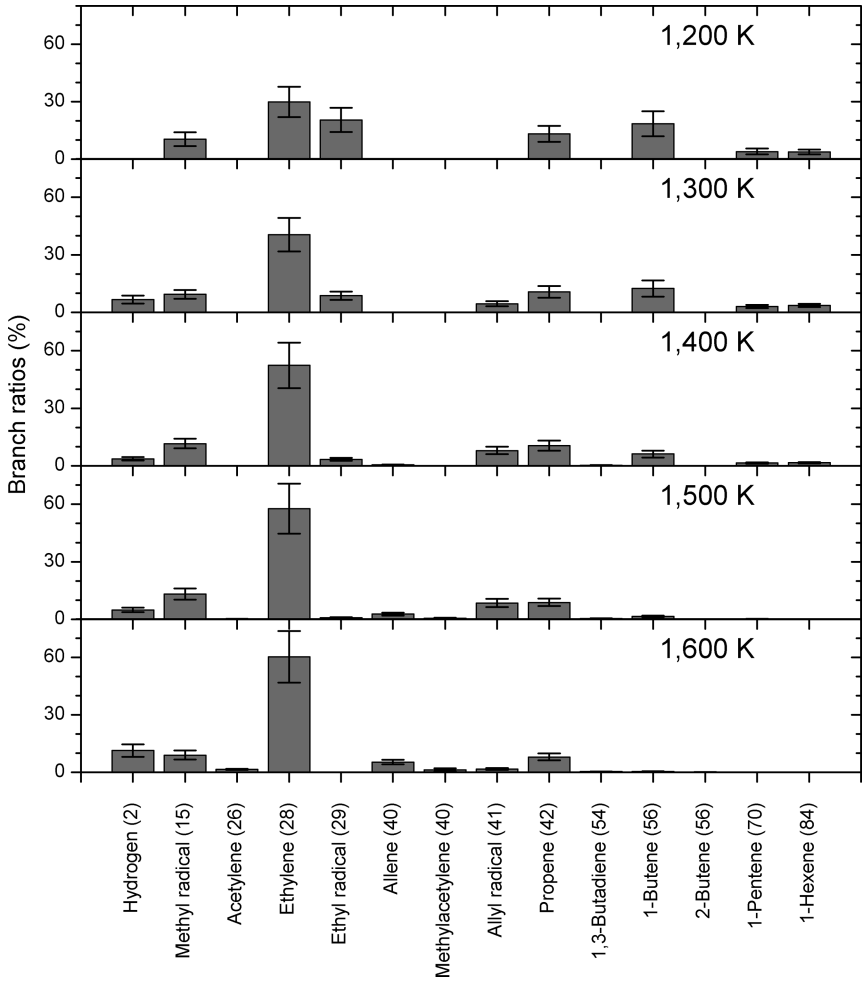

Figure 7. Overall branching ratios of the species obtained in the decomposition of *n*-dodecane in the temperature range from 1200 to 1600 K.

simultaneously the branching ratios of the chemically related ethyl radical (C_2H_5) decrease from about 20% at 1200 K to less than 1% at 1500 K. Acetylene (C_2H_2) represents only minor products of less than 2% at most (1600 K). The initial appearance temperature of acetylene was found to be 1500 K; its branching ratio increases with rising temperature suggesting that acetylene represents one of the final, thermally stable products generated from higher molecular weight intermediates. Besides these C2 products, propene (C_3H_6) with branching ratios slightly decreasing from about 13% (1200 K) to 8% (1600 K) represents the most prominent C3 product. The C3 closed-shell products allene and methylacetylene (C_3H_4) only contribute a total from about 0.6% (1400 K) to 6.7% (1600 K) to the total branching ratios. The C3 radical allyl (C_3H_5) appears at 1300 K. The branching ratio increases from 4% at 1300 K to 9% at 1500 K, and abruptly drops to 2% at 1600 K, suggesting that allyl represents a dynamic intermediate that is simultaneously decomposing while being produced. The branching ratios of the C4 to C7 alkenes steadily decrease as the temperature rises from 1200 to 1600 K indicating that these alkenes decompose in consecutive processes. Therefore, this trend proposes that the C4−C7 hydrocarbons can be classified as reaction intermediates. As a matter of fact, at 1600 K, 1-pentene, 1-hexene, and 1-heptene are completely decomposed and hence undetectable. At 1600 K, among the C4 to C7 products, only 1,3-butadiene (C_4H_6), 1-butene, and 2-butene survive at fractions of less than 1%. Finally, it should be noted that our studies also detected molecular hydrogen (H_2) along with the methyl radical (CH_3). Both of them increase with temperature up to 1500 K, where methyl drops off at 1600 K (the branching ratio of methyl drops from 13% to 9%), while molecular hydrogen keeps increasing.

Finally, the branching ratios as compiled in Table 3 allow us to determine the overall mass balance of the experiments. The overall carbon-to-hydrogen (C/H) ratio is plotted in Figure 8 versus the temperature. The expected C/H ratio of 0.46 is fully recovered at 1200 K suggesting that the mass balance is conserved. At this initial temperature, seven species were observed, with their photoionization cross sections well-defined. The precursor is 40% depleted, and most of carbon and hydrogen elements are still counted from *n*-dodecane. As the temperature rises, the C/H ratios are a little higher than the expected ratio of 0.46. But the theoretical value of 0.46 is still completely covered within the error bars in the entire temperature range.

5. COMPUTATIONAL RESULTS

The *n*-dodecane molecule can decompose by initial cleavage of various C−C (reaction R1) and C−H bonds (reaction R2) producing pairs of 1-alkyl radicals and n-dodecyl radicals plus a hydrogen atom, respectively.

$$C_{12}H_{26} \rightarrow C_xH_y + C_{x'}H_{y'} \quad \text{(R1)}$$

$$C_{12}H_{26} \rightarrow C_{12}H_{25} + H \quad \text{(R2)}$$

DOI: 10.1021/acs.jpca.6b11817
J. Phys. Chem. A 2017, 121, 1281−1297

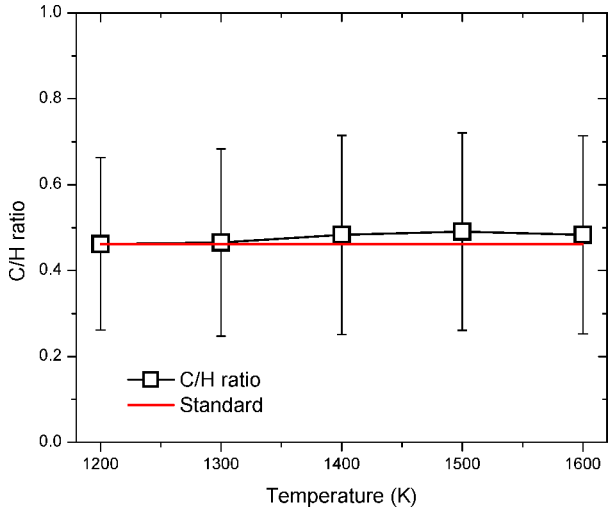

Figure 8. Carbon-to-hydrogen (C/H) ratios in the decomposition of *n*-dodecane in the temperature range from 1200 to 1600 K. Red line defines the standard C/H ratio of *n*-dodecane.

5.1. Homolytic C−C and C−H Bond Cleavages and Consecutive *β*-Scissions (C−C; C−H). The energetics of the C−C bond cleavages in $C_{12}H_{26}$ is illustrated in Figure 9. The C−C bond strengths are calculated to be in the range of 361−366 kJ/mol, where the C2−C3 bond was found to be the weakest and the C5−C6 bond to be the strongest. The differences in the C−C bond strengths are so small that one can anticipate that all product pairs, $CH_3 + C_{11}H_{23}$, $C_2H_5 + C_{10}H_{21}$, $C_3H_7 + C_9H_{19}$, $C_4H_9 + C_8H_{17}$, $C_5H_{11} + C_7H_{15}$, and $C_6H_{13} + C_6H_{13}$, can be in principle formed. On the other hand, the calculated strengths of C−H bonds are significantly higher (Figure 9). The primary C1−H bonds in terminal CH_3 groups are the strongest, 418 kJ/mol, whereas the secondary C−H bonds in CH_2 groups vary in a very narrow range of 406−407 kJ/mol. These values are close to the corresponding experimental C−C and C−H bond strengths in *n*-butane, propane, and ethane evaluated based on enthalpies of formation at 0 K from Active Thermochemical Tables[83] and also to the theoretical values for *n*-decane calculated in our previous work.[45]

Because of the large difference in the bond strengths, rate constants for the C−H cleavages appeared to be several orders of magnitude lower than those for the C−C cleavages and therefore the C−C bond cleavage is predicted to dominate the unimolecular decomposition of dodecane (Figure 10a). In the temperature range of 1000−1600 K and 1 atm, the rate constants for the C−C cleavages exhibit well-defined Arrhenius behavior and grow from 2.6−3.6 s^{-1} to (1−2) × 10^6 s^{-1}. These values agree with the experimental observations that while only a small fraction of *n*-dodecane is consumed at 1100 K, no parent molecules survive above 1500 K during the residence time in the reactor, about tens of microseconds. The computed rate constants for the cleavages of the terminal bonds to produce $CH_3 + C_{11}H_{23}$ are found to be 1-2 orders of magnitude lower than those for the cleavage of nonterminal C−C bonds. The rate

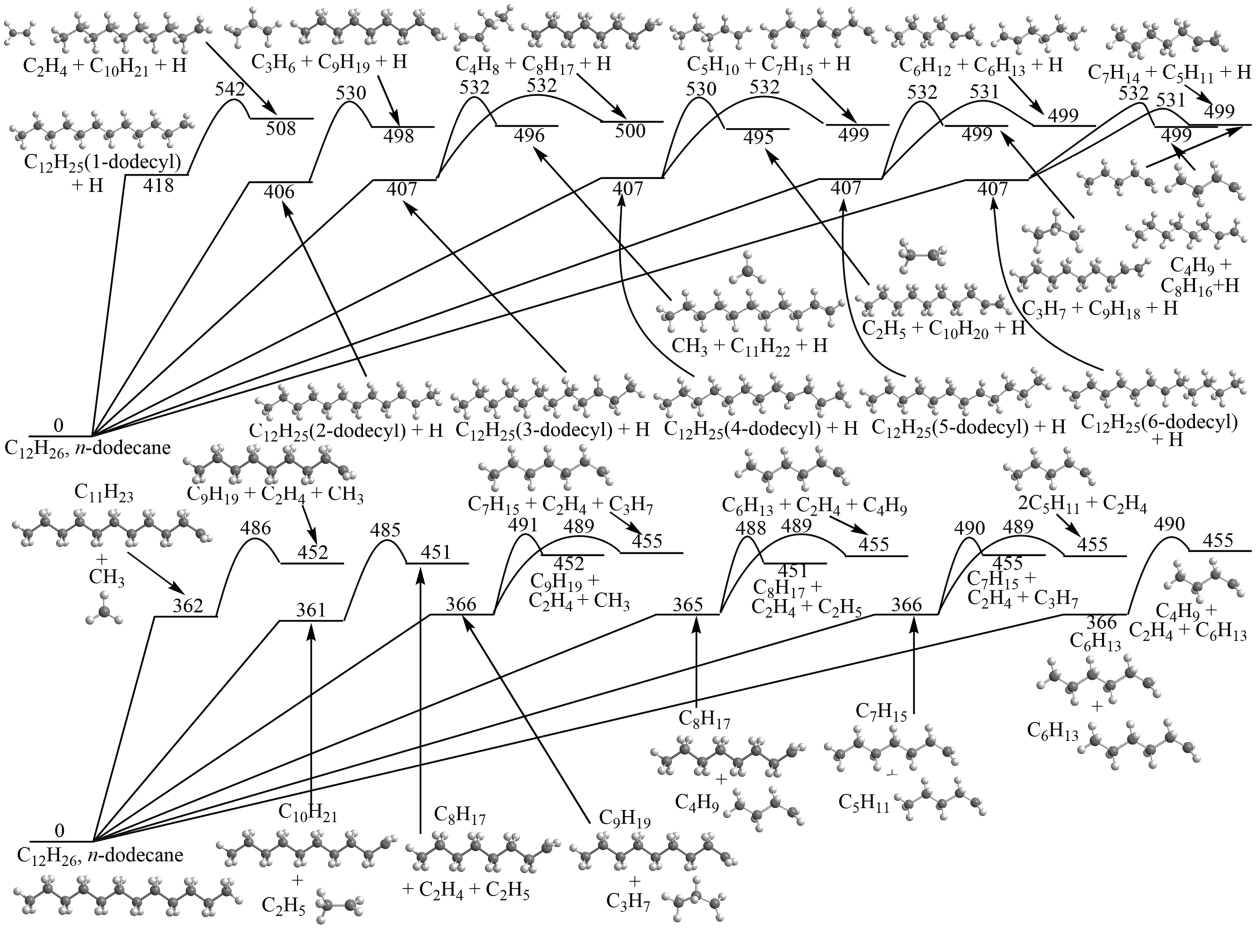

Figure 9. Potential energy diagram for primary and secondary dissociation channels of *n*-dodecane. All relative energies are shown in kJ/mol.

DOI: 10.1021/acs.jpca.6b11817
J. Phys. Chem. A 2017, 121, 1281−1297

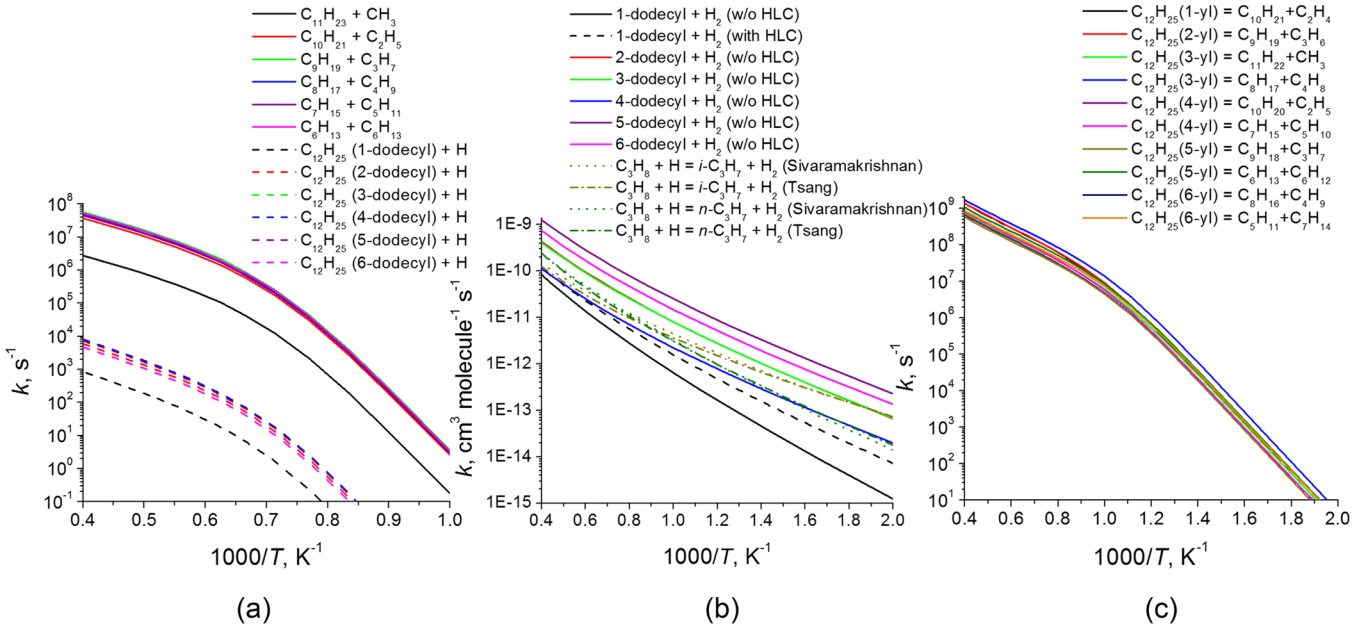

Figure 10. Calculated rate constants (at 1 atm for unimolecular reactions): (a) for C−C and C−H bond cleavages in $C_{12}H_{26}$, (b) for $C_{12}H_{26}$ + H direct H abstractions, and (c) for C−C bond β-scissions in n-dodecyl radicals $C_{12}H_{25}$ (n = 1−6).

constants calculated at 1 atm, except for the one to produce CH_3 + $C_{11}H_{23}$, grow to 4−6 × 10^7 s^{-1} at 2500 K; a small falloff behavior at higher temperatures is seen in a decrease of the slope of the rate constant curves (Figure 10(a)). The computed relative product yields are ∼1% for CH_3 + $C_{11}H_{23}$, 17−16% for C_2H_5 + $C_{10}H_{21}$, 23−24% for C_3H_7 + C_9H_{19}, ∼ 19% for C_4H_9 + C_8H_{17}, 18−19% for C_5H_{11} + C_7H_{15}, and 21−22% for C_6H_{13} + C_6H_{13} and show very slight temperature dependence from 1000 to 2500 K. The product yields are also practically independent of pressure in the range from 30 Torr to 100 atm. This allows us to conclude that the pyrolysis of *n*-dodecane at 1500 K and above should predominantly produce a mixture of 1-alkyl radicals, from ethyl to 1-decyl, on a time scale of 1−2 μs.

In our previous work considering the pyrolysis of *n*-decane[45] we have shown that the higher 1-alkyl radicals are unstable in the experimental temperature range and are subject to a rapid C−C bond β-scission producing ethylene C_2H_4 together with a smaller 1-alkyl. As shown in Figure 9 and Table 6, the calculated barrier heights and reaction energies for the C−C bond β-scissions are 123−126 and 86−92 kJ/mol, respectively. The computed rate constants for C−C bond β-scissions are approximately in the range of 10^7−10^8 s^{-1} at T = 1200−1600 K, and hence, the lifetimes of the primary dissociation products, 1-alkyl radicals, is shorter than 1 μs under the experimental conditions and they are expected to rapidly decompose to the ultimate C_2H_4, CH_3, and C_2H_5 products detected experimentally via the stepwise mechanism shown below. Depending on the residence time, the ethyl radical may or may not further lose an H atom via a C−H bond β-scission producing ethylene.

$$C_{10}H_{21} \rightarrow C_8H_{17} + C_2H_4$$

$$C_9H_{19} \rightarrow C_7H_{15} + C_2H_4$$

$$C_8H_{17} \rightarrow C_6H_{13} + C_2H_4$$

$$C_7H_{15} \rightarrow C_5H_{11} + C_2H_4$$

$$C_6H_{13} \rightarrow C_4H_9 + C_2H_4$$

Table 6. Calculated Barrier Heights and Reaction Energies for Various C−C Bond β-Scission and Direct H Abstraction Reactions

reactions	barrier (kJ/mol)	reaction energy (kJ/mol)
$C_{11}H_{23} \rightarrow C_9H_{19} + C_2H_4$	124	90
$C_{10}H_{21} \rightarrow C_8H_{17} + C_2H_4$	123	89
$C_9H_{19} \rightarrow C_7H_{15} + C_2H_4$	124	89
$C_8H_{17} \rightarrow C_6H_{13} + C_2H_4$	124	92
$C_7H_{15} \rightarrow C_5H_{11} + C_2H_4$	124	91
$C_6H_{13} \rightarrow C_4H_9 + C_2H_4$	124	89
$C_5H_{11} \rightarrow C_3H_7 + C_2H_4$	124	89
$C_4H_9 \rightarrow C_2H_5 + C_2H_4$	123	86
$C_3H_7 \rightarrow CH_3 + C_2H_4$	126	86
$C_{12}H_{25}$ (1-dodecyl) → $C_{10}H_{21} + C_2H_4$	124	90
$C_{12}H_{25}$ (2-dodecyl) → $C_9H_{19} + C_3H_6$	124	92
$C_{12}H_{25}$ (3-dodecyl) → $C_{11}H_{22} + CH_3$	125	89
$C_{12}H_{25}$ (3-dodecyl) → $C_8H_{17} + C_4H_8$	125	93
$C_{12}H_{25}$ (4-dodecyl) → $C_{10}H_{20} + C_2H_5$	123	88
$C_{12}H_{25}$ (4-dodecyl) → $C_5H_{10} + C_7H_{15}$	125	93
$C_{12}H_{25}$ (5-dodecyl) → $C_9H_{18} + C_3H_7$	125	92
$C_{12}H_{25}$ (5-dodecyl) → $C_6H_{12} + C_6H_{13}$	125	93
$C_{12}H_{25}$ (6-dodecyl) → $C_7H_{14} + C_5H_{11}$	125	92
$C_{12}H_{25}$ (6-dodecyl) → $C_8H_{16} + C_4H_9$	125	92
$C_{12}H_{26}$ + H → $C_{12}H_{25}$ (1-dodecyl) + H_2	49 (42)[a]	−12 (−19)[a]
$C_{12}H_{26}$ + H → $C_{12}H_{25}$ (2-dodecyl) + H_2	36 (28)[a]	−24 (−31)[a]
$C_{12}H_{26}$ + H → $C_{12}H_{25}$ (3-dodecyl) + H_2	36 (28)[a]	−23 (−30)[a]
$C_{12}H_{26}$ + H → $C_{12}H_{25}$ (4-dodecyl) + H_2	35 (28)[a]	−23 (−31)[a]
$C_{12}H_{26}$ + H → $C_{12}H_{25}$ (5-dodecyl) + H_2	35 (27)[a]	−23 (−31)[a]
$C_{12}H_{26}$ + H → $C_{12}H_{25}$ (6-dodecyl) + H_2	35 (27)[a]	−23 (−30)[a]

[a]The values including the higher level correction (HLC) for H abstractions are given in parentheses.

$$C_5H_{11} \rightarrow C_3H_7 + C_2H_4$$

$$C_4H_9 \rightarrow C_2H_5 + C_2H_4$$

$$C_3H_7 \rightarrow CH_3 + C_2H_4$$

DOI: 10.1021/acs.jpca.6b11817
J. Phys. Chem. A 2017, 121, 1281−1297

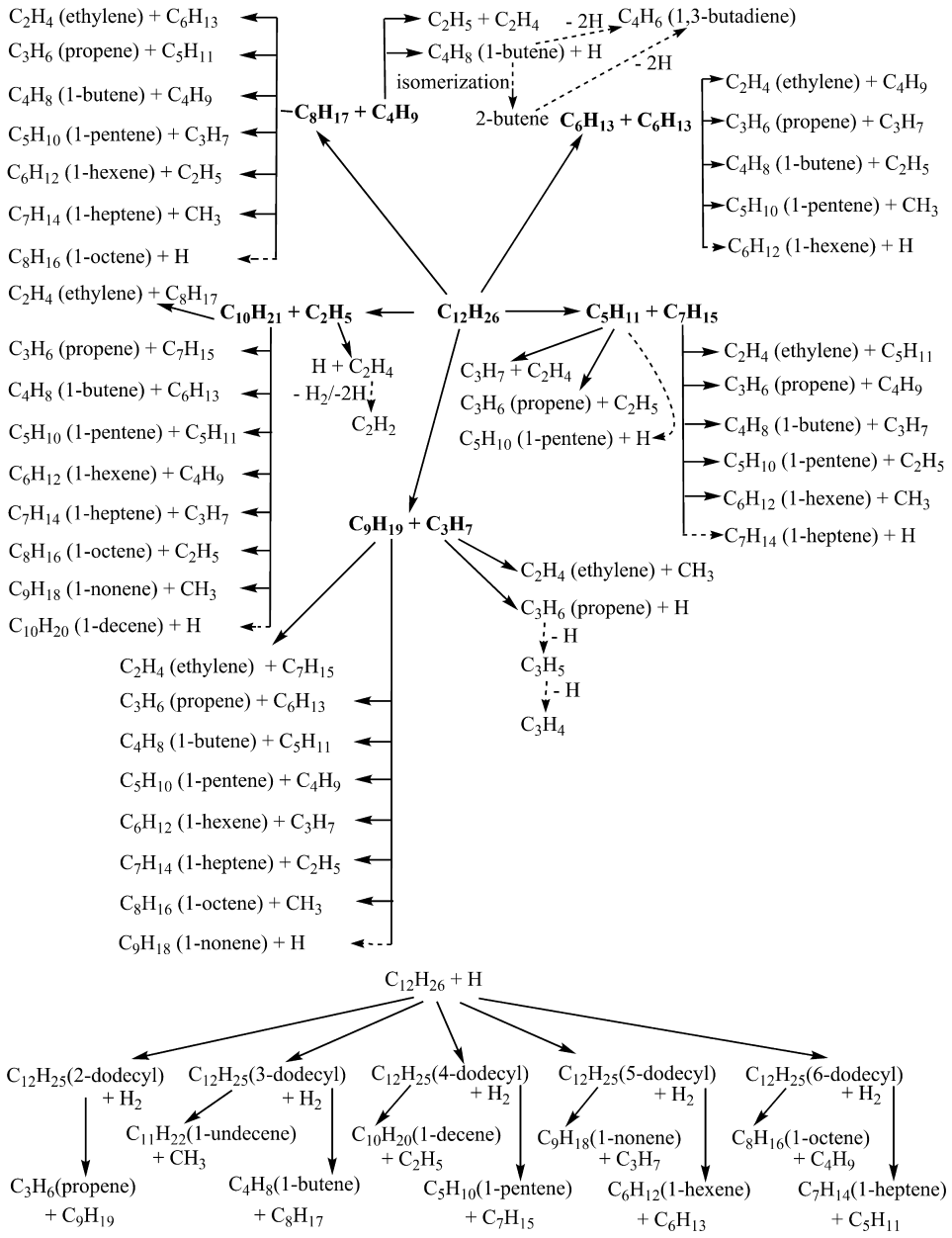

Figure 11. Proposed reaction mechanism for the pyrolysis of *n*-dodecane.

$$C_2H_5 \rightarrow H + C_2H_4$$

The mechanism of consecutive direct C−C bond β-scissions unzipping large 1-alkyl radicals down to the mixture of C_2H_4, C_2H_5, and CH_3 cannot explain the experimental observation of higher 1-alkenes, especially propene and 1-butene, which are among major pyrolysis products at 1200 K and are still present up to 1600 K. We discussed several possible formation pathways of 1-alkenes in the previous paper on *n*-decane.[45] The first one is C−H bond β-scission in 1-alkyls, but according to the calculations C−H β-scission barriers are 20−26 kJ/mol higher than the corresponding C−C β-scission barriers in C_3H_7−C_8H_{17}. Because of this difference, the computed branching ratios for the C−H β-scission channels in C_4H_9−C_8H_{17} are very small and do not exceed 1−2% until the highest temperatures and pressures (2500 K and 100 atm), where they reach 5−6%.[45] The relative yield of propene + H is higher from C_3H_7 and increases from 3 to 4% at 1100−1600 K and 1 atm to 6%, 9%, and 13% at 2500 K and pressures of 1, 10, and 100 atm, respectively. Thus, C−H bond β-scissions cannot explain the large experimental yields of propene and 1-butene since they are largely unfavorable compared to the β-scissions with the loss of C_2H_4. Summarizing, C−C bond cleavages leading to 1-alky radicals are strongly favored compared to C−H bond rupture processes; the higher 1-alkyl radicals (>C2) do not survive under our experimental conditions and decay via successive C−C β-scissions (C_2H_4 elimination), which dominate over C−H β-scission (alkene formation), to yield eventually the C1 to C2 hydrocarbons CH_3, C_2H_5, and C_2H_4.

5.2. Hydrogen Migrations and Consecutive β-Scissions. The second possible mechanism to form higher alkenes involves H atom shifts in 1-alkyl radicals followed by C−C bond β-scission. We have shown[45] that isomerization channels involving 1,2- and 1,3-H atom shifts in C_3H_7 and C_4H_9 are not competitive due to their high barriers of 157−162 kJ/mol significantly exceeding the C−C bond β-scission barriers of

DOI: 10.1021/acs.jpca.6b11817
J. Phys. Chem. A 2017, 121, 1281−1297

~124 kJ/mol. On the other hand, a possibility of 1,4-H, 1,5-H, 1,6-H, and 1,7-H shifts eventually opens up in higher 1-alkyl radicals beginning from C_5H_{11} and the corresponding typical barriers for these processes, 92−94, 64−66, 71−72, and 80 kJ/mol, respectively, are *lower* than those for the C−C bond β-scission. The hydrogen shifts are followed by C−C β-scissions forming higher 1-alkenes rather than ethylene, i.e., propene (C_3H_6), 1-butene (C_4H_8), 1-pentene (C_5H_{10}), and so on, depending on the radical position in the alkyl. We calculated and reported product branching ratios in dissociation of 1-alkyl radicals C_5H_{11}−C_8H_{17} taking into account direct C−C and C−H β-scissions as well as all C−C β-scissions following the H shifts in the previous work[45] and demonstrated that at low pressures up to 1 atm, the products formed after a 1,5-H shift are preferable, but at high pressures of 10 and 100 atm, the direct C−C β-scission from 1-alkyls producing ethylene (C_2H_4) dominates. Nevertheless, various alkenes can be formed from the 1-alkyl radicals with non-negligible branching ratios, e.g., from C_5H_{11}: C_3H_7 + C_2H_4 (direct), C_2H_5 + C_3H_6 (via 1,4-H shift and 2-pentyl); from C_6H_{13}: C_4H_9 + C_2H_4 (direct), C_3H_7 + C_3H_6 (via 1,5-H shift and 2-hexyl), CH_3 + C_5H_{10} and C_2H_5 + C_4H_8 (both via 1,4-H shift and 3-hexyl); etc. (see Figure 11 for the full list of possible products from 1-alkyls C_3H_7−$C_{10}H_{21}$). As compared with *n*-decane, *n*-dodecane has two higher 1-alkyl radicals among its primary products, 1-nonyl (C_9H_{19}) and 1-decyl ($C_{10}H_{21}$). While one can expect that the barriers for 1,4-, 1,5-, 1,6-, and 1,7-H shifts should retain their typical values in C_9H_{19} and $C_{10}H_{21}$ and hence the corresponding H shift/C−C β-scission channels would remain competitive, new reaction channels may additionally open up, 1,8-H shifts both in 1-nonyl and 1-decyl and 1,9-H shift in 1-decyl. Here, we evaluated the 1,8- and 1,9-H shift barriers in $C_{10}H_{21}$. The calculation gave the values of 97 and 90 kJ/mol, respectively. While these barriers are higher than those for 1,5-, 1,6-, and 1,7-H shifts, and are comparable to 1,4-H shifts, they are still somewhat lower than the barrier for the direct C−C β-scission. Therefore, the dissociation channels involving the 1,8- and 1,9-H shifts followed by C−C β-scissions can give minor contributions to the overall product yield. In particular, 1-nonyl can isomerize to 2-nonyl by 1,8-H shift and then decompose to C_6H_{13} + C_3H_6. 1-Decyl can isomerize to 2-decyl by 1,9-shift and dissociate to C_7H_5 + C_3H_6 or isomerize to 3-decyl and decompose to either CH_3 + C_9H_{18} or C_6H_{13} + C_4H_8. Summarizing, the reaction mechanism involving hydrogen migration in C5 to C10 1-alkyl radicals preceding C−C β-scission accounts for the observation of C3−C7 alkenes [propene, 1-butene, 1-pentene, 1-hexene, and 1-heptene] observed in our experiments and, in particluar, for the large branching ratios of C_3H_6 and C_4H_8 at low temperatures (and even at 1600 K for propene). At temperatures of 1500 K and above the lifetime of a single C−C bond approaches 1 μs and hence higher alkenes are likely to decompose on the time scale of the experiment and their yield significantly decrease.

5.3. Hydrogen Abstraction. The third possible pathway to the higher alkenes involves C−C bond β-scissions in n-dodecyl radicals (n > 1; see Figure 9 and Table 6). While n-dodecyls are not expected to be formed by C−H bond cleavages in *n*-dodecane, they can be produced by direct hydrogen abstractions by H atoms or other radicals when those radicals appear in the reactive system. The barrier heights and reaction exoergicities for the H abstraction reactions by a hydrogen atom from secondary C−H bonds are computed to be 35−36 (27−28) and 23−24 (30−31) kJ/mol; the numbers in parentheses include HLC in the G3(CCSD,MP2) calculations. The H abstractions from the primary C−H bonds exhibit a higher barrier and a lower reaction exoergicity of 49 (42) and 12 (19) kJ/mol, respectively. These results are close to the corresponding values obtained in the previous work for *n*-decane.[45] Note that, the most accurate up-to-date calculations of H abstraction from C_3H_8 and C_2H_6 gave the reaction barriers and exoergicities as 32 and 27 kJ/mol, respectively, for the secondary hydrogen abstraction and 43−44 and 15−16 kJ/mol for the primary hydrogen abstraction.[84] The calculated rate constants for secondary H abstractions are generally higher than those for the primary hydrogen abstraction (Figure 10b) and, among secondary H abstractions, the reaction producing 5-dodecyl is preferred and followed by the reactions giving 5-dodecyl, then by 2- and 3-dodecyl (with similar rate constants), and finally by 4-dodecyl. The computed rate constants to form 2- and 3-dodecyl agree best with the literature data (the most accurate calculations for C_3H_8[84] and experimental data for C_3H_8, C_4H_{10}, and C_5H_{12}[85,86]) for the secondary H abstraction at 500 K but overestimate the literature data at 2500 K by approximately a factor of 3. Alternatively, the rate constants for the production of 4-dodecyl agree closely with the literature values at high temperatures. Our results indicate that the rate constants for secondary H abstraction are sensitive to the attacked hydrogen atom position in the alkane. It should be noted however that a more rigorous anharmonic treatment of soft normal modes would be required to generate quantitatively accurate H abstraction rate constants. For the primary hydrogen abstraction, the $C_{12}H_{26}$ + H rate constants underestimate those for C_3H_8 + H by 50−60% if HLC is taken into account; the difference is bigger if the correction is not included.

Our main conclusion is that the secondary H abstractions are feasible and form n-dodecyl radicals (n > 1). Once the n-dodecyl radicals are produced, they can rapidly undergo C−C bond β-scission to yield higher alkenes together with 1-alkyl radicals:

$$C_{12}H_{25}(2\text{-dodecyl}) \rightarrow C_3H_6 + C_9H_{19}$$

$$C_{12}H_{25}(3\text{-dodecyl}) \rightarrow C_{11}H_{22} + CH_3$$
$$\rightarrow C_4H_8 + C_8H_{17}$$

$$C_{12}H_{25}(4\text{-dodecyl}) \rightarrow C_{10}H_{20} + C_2H_5$$
$$\rightarrow C_5H_{10} + C_7H_{15}$$

$$C_{12}H_{25}(5\text{-dodecyl}) \rightarrow C_9H_{18} + C_3H_7$$
$$\rightarrow C_6H_{12} + C_6H_{13}$$

$$C_{12}H_{25}(6\text{-dodecyl}) \rightarrow C_7H_{14} + C_5H_{11}$$
$$\rightarrow C_8H_{16} + C_4H_9$$

The calculated barriers for these reactions are 123−125 kJ/mol and they are endoergic by 88−93 kJ/mol; these energetic parameters are thus similar to those for C−C β-scissions in smaller alkyl radicals considered above and in the previous work.[45] The rate constants calculated at 1 atm are close for all the reactions considered within a factor of 2 (Figure 10c). The results indicate that the lifetime of the dodecyl varies in the 5−50 ns range under the experimental conditions. Summarizing, n-dodecyl radicals, which may be produced by hydrogen abstraction, can also undergo subsequent C−C bond β-scissions leading to experimentally observed alkenes: 1-butene, 1-pentene, 1-hexene, and 1-heptene.

DOI: 10.1021/acs.jpca.6b11817
J. Phys. Chem. A 2017, 121, 1281−1297

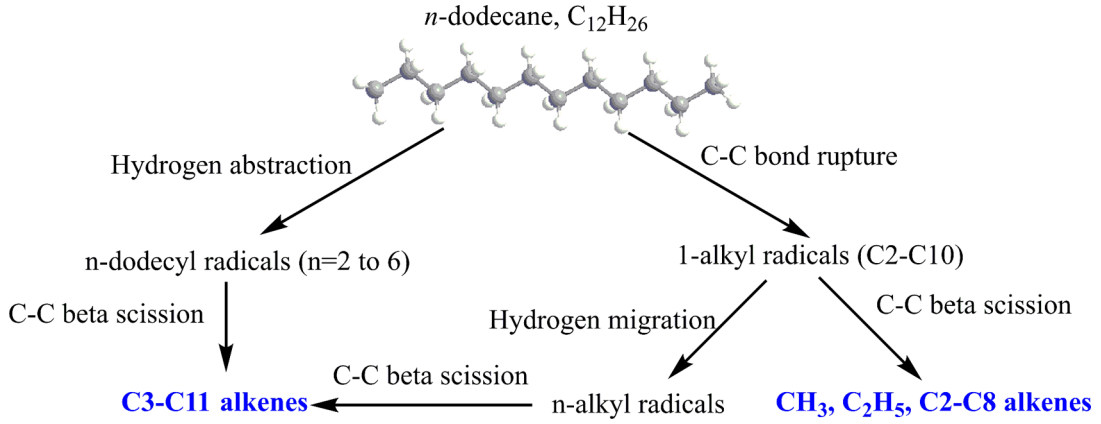

Figure 12. Summary of reaction mechanisms leading to primary reaction products in the decomposition of *n*-dodecane.

6. DISCUSSION AND CONCLUSION

We combine now the experimental results with the electronic structure and rate constant calculations with the goal to elucidate the (predominant) temperature-dependent decomposition pathways. The compiled mechanism of the pyrolysis is illustrated in Figures 11 and 12.

1 At the initial stage, *n*-dodecane dissociates by C−C bond cleavages (excluding the terminal C−C bonds) and produces $C_{10}H_{21}$ + C_2H_5, C_9H_{19} + C_3H_7, C_8H_{17} + C_4H_9, C_7H_{15} + C_5H_{11}, and C_6H_{13} + C_6H_{13}, i.e., a mixture of C2 to C10 1-alkyl radicals from ethyl to 1-decyl.

2 The alkyl radicals are unstable under the experimental conditions. They rapidly dissociate by two possible mechanisms: (a) C−C bond β-scissions to split ethylene (C_2H_4) plus a 1-alkyl radical with the number of carbon atoms reduced by two and (b) 1,4-, 1,5-, 1,6-, 1,7-, 1,8-, or 1,9-H shifts followed by C−C β-scission producing alkenes from propene to 1-nonene in combination with smaller 1-alkyl radicals. The higher alkenes become increasingly unstable as the temperatures rises and the yield of propene and 1-butene, large at 1200 K, decreases. When the C−C β-scission continues all the way to the propyl radical, C_3H_7, it dissociates producing CH_3 + C_2H_4. This mechanism allows us to explain the appearance of the predominant pyrolysis products, ethylene (C_2H_4), methyl (CH_3), ethyl (C_2H_5), propene (C_3H_6), and 1-butene (C_4H_8), as well as small yields of 1-pentene (C_5H_{10}), 1-hexene (C_6H_{12}), and 1-heptene (C_7H_{14}). The higher yield of the ethyl radical here as compared to *n*-decane may be related to the fact that a larger amount of higher 1-alkyl radicals is formed among the primary decomposition products of *n*-dodecane. These higher 1-alkyls require more C−C β-scission steps and hence a longer time to reach C_2H_5. Consequently, a larger fraction of the C_2H_5 radicals survives and does not dissociate to C_2H_4 + H before leaving the reactor.

3 At higher temperatures, hydrogen atoms can abstract hydrogen from $C_{12}H_{26}$ to yield n-dodecyl radicals. The n-dodecyl radicals can dissociate via C−C bond β-scissions to C3−C11 alkenes. Hydrogen migration and β-scissions of radicals are important reactions in hydrocarbon decomposition.[87,88]

4 The other trace products, which account for a maximum of about 10%, can only be produced via higher order reactions. For instance, acetylene C_2H_2 can be formed via unimolecular decomposition of C_2H_4 by sequential losses of two H atoms or by H_2 elimination.[89] In contrast to the *n*-decane pyrolysis,[45] we have not observed the vinyl radical C_2H_3 here, although it can be in principle formed by H loss from C_2H_4 or via a single C−C bond cleavage in higher alkenes. Apparently, the yield of C_2H_3 is too low for this radical to be detected in this work. The allyl radical C_3H_5 can be formed by the primary C−H bond cleavage in propene or a single C−C bond cleavage in higher alkenes:

$$C_3H_6 \rightarrow C_3H_5 + H$$

$$C_4H_8 \rightarrow C_3H_5 + CH_3$$

$$C_5H_{10} \rightarrow C_3H_5 + C_2H_5$$

$$C_6H_{12} \rightarrow C_3H_5 + C_3H_7$$

The allyl radical is well-known to eventually decompose to allene, to methylacetylene (C_3H_4), and eventually to the propargyl radical C_3H_3.[90−92] Propargyl was not detected in the present experiment, indicating that its yield was too small. At last, 2-butene can be formed by isomerization of 1-butene[93] and 1,3-butadiene is a major dissociation product of the C_4H_7 radical,[94] which in turn can be produced by C−H bond cleavage in 1-butene[92] or by C−C bond cleavage in higher alkenes starting from 1-pentene.

Comparing the results of the present experiment with those from previous experimental studies, it should be noted that the earlier investigations were mostly limited to the identification of closed-shell hydrocarbon intermediates and products because the decomposition products were derived mainly from off-line and *ex situ* (HPLC, GC MS) analysis. This approach disallowed the detection of thermally unstable intermediates and hydrocarbon radicals. This limitation has been overcome in the present investigation since photoionization of the decomposition products online and *in situ* is a solid and versatile experimental tool allowing the detection of a full set of decomposition products including both thermally stable and unstable species, such as radicals. Additionally, we observed the decomposition products on the microsecond time scale, meaning that the initial decomposition products were detected. In previous experiments in the reactors and shock tubes, residence time scales were in the order of a few milliseconds (Table 1) and thermally unstable products, especially, radicals are not likely to survive, although they may have been formed initially. Therefore, the present study provides a most complete record of radicals and other thermally

DOI: 10.1021/acs.jpca.6b11817
J. Phys. Chem. A 2017, 121, 1281−1297

unstable species produced in the initial stage of decomposition and thus de facto characterizes the radical pool available for further oxidation of the fuel, which is required for generation of accurate kinetic models of combustion of aviation fuels. Also, the short residence time used in the present work effectively excludes undesired mass growth processes. Finally, the combined experimental and theoretical studies of *n*-dodecane and earlier,[45] of *n*-decane allowed us to reveal and clearly formulate the chemical mechanism of the pyrolysis of large *n*-alkane molecules, which represent the major fuel components.

■ ASSOCIATED CONTENT

Supporting Information

The Supporting Information is available free of charge on the ACS Publications website at DOI: 10.1021/acs.jpca.6b11817.

Table S1, detected molecules in previous experimental studies of *n*-dodecane pyrolysis; and Table S2. parameters of the fitted modified Arrhenius expressions for most important reactions involved in pyrolysis of *n*-dodecane (PDF)

■ AUTHOR INFORMATION

Corresponding Authors

*(R.I.K.) E-mail: ralfk@hawaii.edu.
*(M.A.) E-mail: mahmed@lbl.gov.
*(A.M.M.) E-mail: mebela@fiu.edu.

ORCID

Tao Yang: 0000-0003-4101-2385
Ralf I. Kaiser: 0000-0002-7233-7206
Alexander M. Mebel: 0000-0002-7233-3133

Notes

The authors declare no competing financial interest.

■ ACKNOWLEDGMENTS

This project is supported by the Air Force Office of Scientific Research (AFOSR) under Grant Number FA9550-15-1-0011 (L.Z., T.Y., R.I.K., A.M.M.) to the University of Hawaii and Florida International University. T.P.T. and M.A. along with the Advanced Light Source are supported by the Director, Office of Science, Office of Basic Energy Sciences, of the U.S. Department of Energy, under Contract No. DE-AC02-05CH11231, through the Chemical Sciences Division. J.M.R. thanks FIU Graduate School for his Doctoral Evidence Acquisition Fellowship.

■ REFERENCES

(1) Bruno, T. J.; Abel, K. R.; Riggs, J. R. Comparison of JP-8 and JP-8 + 100 with the Advanced Distillation Curve Approach. *Energy Fuels* **2012**, *26*, 5843−5850.

(2) Bezaire, N.; Wadumesthrige, K.; Simon Ng, K. Y.; Salley, S. O. Limitations of the Use of Cetane Index for Alternative Compression Ignition Engine Fuels. *Fuel* **2010**, *89*, 3807−3813.

(3) Gregg, S. D.; Campbell, J. L.; Fisher, J. W.; Bartlett, M. G. Methods for the Characterization of Jet Propellent-8: Vapor and Aerosol. *Biomed. Chromatogr.* **2007**, *21*, 463−472.

(4) Gough, R. V.; Bruno, T. J. Composition-Explicit Distillation Curves of Alternative Turbine Fuels. *Energy Fuels* **2013**, *27*, 294−302.

(5) Meylemans, H. A.; Baldwin, L. C.; Harvey, B. G. Low-Temperature Properties of Renewable High-Density Fuel Blends. *Energy Fuels* **2013**, *27*, 883−888.

(6) Witten, M. L.; Zeiger, E.; Ritchie, G. D. *Jet Fuel Toxicology*; CRC Press: 2011.

(7) Rodgers, R. P.; Blumer, E. N.; Freitas, M. A.; Marshall, A. G. Jet Fuel Chemical Composition, Weathering, and Identification as a Contaminant at a Remediation Site, Determined by Fourier Transform Ion Cyclotron Resonance Mass Spectrometry. *Anal. Chem.* **1999**, *71*, 5171−5176.

(8) DuBois, T. G.; Nieh, S. In *Effects of Hydrocarbon Chemical Class Composition on Autothermal Reforming of JP-8 Fuel*, Presented at the Power Sources Conference, Las Vegas, Nevada, USA, Jun. 14−17.

(9) Echavarria, C. A.; Jaramillo, I. C.; Sarofim, A. F.; Lighty, J. S. Burnout of Soot Particles in a Two-Stage Burner With a JP-8 Surrogate Fuel. *Combust. Flame* **2012**, *159*, 2441−2448.

(10) Wang, H.; Oehlschlaeger, M. A. Autoignition Studies of Conventional and Fischer−Tropsch Jet Fuels. *Fuel* **2012**, *98*, 249−258.

(11) Merrill, E. A.; Gearhart, J. M.; Sterner, T. R.; Robinson, P. J. Improved Predictive Model for *n*-Decane Kinetics Across Species, as a Component of Hydrocarbon Mixtures. *Inhalation Toxicol.* **2008**, *20*, 851−63.

(12) Holley, A. T.; Dong, Y.; Andac, M. G.; Egolfopoulos, F. N.; Edwards, T. Ignition and Extinction of Non-Premixed Flames of Single-Component Liquid Hydrocarbons, Jet Fuels, and Their Surrogates. *Proc. Combust. Inst.* **2007**, *31*, 1205−1213.

(13) Pitz, W. J.; Cernansky, N. P.; Dryer, F. L.; Egolfopoulos, F. N.; Farrell, J. T.; Friend, D. G.; Pitsch, H. *Development of an Experimental Database and Chemical Kinetic Models for Surrogate Gasoline Fuels*; SAE International: 2007.

(14) Allen, C.; Valco, D.; Toulson, E.; Edwards, T.; Lee, T. Ignition Behavior and Surrogate Modeling of Jp-8 and of Camelina and Tallow Hydrotreated Renewable Jet Fuels at Low Temperatures. *Combust. Flame* **2013**, *160*, 232−239.

(15) Natelson, R. H.; Kurman, M. S.; Johnson, R. O.; Cernansky, N. P.; Miller, D. L. Preignition and Autoignition Chemistry of the Xylene Isomers. *Combust. Sci. Technol.* **2011**, *183*, 897−914.

(16) Joklik, R.; Fuller, C.; Turner, B.; Gokulakrishnan, P. The Effect of Multi-Component Fuel Evaporation on the Ignition of JP-8. In *ASME Turbo Expo 2010: Power for Land, Sea, and Air*; 2010.

(17) Honnet, S.; Seshadri, K.; Niemann, U.; Peters, N. A Surrogate Fuel for Kerosene. *Proc. Combust. Inst.* **2009**, *32*, 485−492.

(18) Tosatto, L.; Mantia, B. L.; Bufferand, H.; Duchaine, P.; Gomez, A. Chemical Structure of a Methane Counterflow Diffusion Flame Perturbed with the Addition of either JP-8 or a Jet Fuel Surrogate. *Proc. Combust. Inst.* **2009**, *32*, 1319−1326.

(19) Lenhert, D. B.; Miller, D. L.; Cernansky, N. P. The Oxidation of JP-8, Jet-A, and Their Surrogates in the Low and Intermediate Temperature Regime at Elevated Pressures. *Combust. Sci. Technol.* **2007**, *179*, 845−861.

(20) Kahandawala, M. S. P.; DeWitt, M. J.; Corporan, E.; Sidhu, S. S. Ignition and Emission Characteristics of Surrogate and Practical Jet Fuels. *Energy Fuels* **2008**, *22*, 3673−3679.

(21) Katta, V. R.; Roquemore, W. M. In Performance of JP-8 Surrogates and Parent Species in a Swirl Combustor. In *ASME Turbo Expo 2010: Power for Land, Sea, and Air*; 2010.

(22) Ji, C.; Sarathy, S. M.; Veloo, P. S.; Westbrook, C. K.; Egolfopoulos, F. N. Effects of Fuel Branching on the Propagation of Octane Isomers Flames. *Combust. Flame* **2012**, *159*, 1426−1436.

(23) Natelson, R. H.; Johnson, R. O.; Kurman, M. S.; Cernansky, N. P.; Miller, D. L. Comparison of Reactivity in a Flow Reactor and a Single Cylinder Engine. *Exp. Therm. Fluid Sci.* **2010**, *34*, 928−932.

(24) Caton, P. A.; Hamilton, L. J.; Cowart, J. S. Understanding Ignition Delay Effects With Pure Component Fuels in a Single-Cylinder Diesel Engine. *J. Eng. Gas Turbines Power* **2011**, *133*, 032803.

(25) Tosatto, L.; Mella, F.; Long, M. B.; Smooke, M. D. A Study of JP-8 Surrogate Coflow Flame Structure by Combined Use of Laser Diagnostics and Numerical Simulation. *Combust. Flame* **2012**, *159*, 3027−3039.

(26) Mawid, M. A.; Park, T. W.; Sekar, B.; Arana, C. *Development and Validation of A Detailed JP-8 Fuel Chemistry Model*. Presented at the 2nd JANNAF Modeling and Simulation Subcommittee Meeting, Destin, FL.

(27) Miller, J. A.; Pilling, M. J.; Troe, J. Unravelling Combustion Mechanisms Through a Quantitative Understanding of Elementary Reactions. *Proc. Combust. Inst.* **2005**, *30*, 43−88.

DOI: 10.1021/acs.jpca.6b11817
J. Phys. Chem. A 2017, 121, 1281−1297

(28) Violi, A.; Yan, S.; Eddings, E. G.; Sarofim, F.; Granata, S.; Faravelli, T.; Ranzi, E. Experimental Formulation and Kinetic Model for JP-8 Surrogate Mixtures. *Combust. Sci. Technol.* **2002**, *174*, 399−417.
(29) Podlesak, T.; Hendrickson, M.; Matthews, S.; Nawrocki, E.; Seibert, M.; Zalewski, M. Army Stirling Engine Research and Development - Past, Present and Future. *Power Sources Conference* **2010**, *44*, 462−465.
(30) Malewicki, T.; Brezinsky, K. Experimental and Modeling Study on the Pyrolysis and Oxidation of *n*-Decane and *n*-Dodecane. *Proc. Combust. Inst.* **2013**, *34*, 361−368.
(31) MacDonald, M. E.; Ren, W.; Zhu, Y.; Davidson, D. F.; Hanson, R. K. Fuel and Ethylene Measurements During *n*-Dodecane, Methylcyclohexane, and *iso*-Cetane Pyrolysis in Shock Tubes. *Fuel* **2013**, *103*, 1060−1068.
(32) Banerjee, S.; Tangko, R.; Sheen, D. A.; Wang, H.; Bowman, C. T. An Experimental and Kinetic Modeling Study of *n*-Dodecane Pyrolysis and Oxidation. *Combust. Flame* **2016**, *163*, 12−30.
(33) Dahm, K. D.; Virk, P. S.; Bounaceur, R.; Battin-Leclerc, F.; Marquaire, P. M.; Fournet, R.; Daniau, E.; Bouchez, M. Experimental and Modelling Investigation of the Thermal Decomposition of *n*-Dodecane. *J. Anal. Appl. Pyrolysis* **2004**, *71*, 865−881.
(34) Herbinet, O.; Marquaire, P. M.; Battin-Leclerc, F.; Fournet, R. Thermal Decomposition of *n*-Dodecane: Experiments and Kinetic Modeling. *J. Anal. Appl. Pyrolysis* **2007**, *78*, 419−429.
(35) Zhou, P. H.; Hollis, O. L.; Crynes, B. L. Thermolysis of Higher Molecular-Weight Straight-Chain Alkanes C9-C22. *Ind. Eng. Chem. Res.* **1987**, *26*, 846−852.
(36) Yu, J.; Eser, S. Thermal Decomposition of C10-C14 Normal Alkanes in Near-Critical and Supercritical Regions: Product Distributions and Reaction Mechanisms. *Ind. Eng. Chem. Res.* **1997**, *36*, 574−584.
(37) Yu, J.; Eser, S. Kinetics of Supercritical-Phase Thermal Decomposition of C10-C14 Normal Alkanes and Their Mixtures. *Ind. Eng. Chem. Res.* **1997**, *36*, 585−591.
(38) Ranzi, E.; Frassoldati, A.; Granata, S.; Faravelli, T. Wide-Range Kinetic Modeling Study of the Pyrolysis, Partial Oxidation, and Combustion of Heavy *n*-Alkanes. *Ind. Eng. Chem. Res.* **2005**, *44*, 5170−5183.
(39) Stagni, A.; Cuoci, A.; Frassoldati, A.; Faravelli, T.; Ranzi, E. Lumping and Reduction of Detailed Kinetic Schemes: an Effective Coupling. *Ind. Eng. Chem. Res.* **2014**, *53*, 9004−9016.
(40) Biet, J.; Hakka, M. H.; Warth, V.; Glaude, P. A.; Battin-Leclerc, F. Experimental and Modeling Study of the Low-Temperature Oxidation of Large Alkanes. *Energy Fuels* **2008**, *22*, 2258−2269.
(41) You, X. Q.; Egolfopoulos, F. N.; Wang, H. Detailed and Simplified Kinetic Models of *n*-Dodecane Oxidation: The Role of Fuel Cracking in Aliphatic Hydrocarbon Combustion. *Proc. Combust. Inst.* **2009**, *32*, 403−410.
(42) Dooley, S.; Won, S. H.; Chaos, M.; Heyne, J.; Ju, Y.; Dryer, F. L.; Kumar, K.; Sung, C.-J.; Wang, H.; Oehlschlaeger, M. A.; et al. A Jet Fuel Surrogate Formulated by Real Fuel Properties. *Combust. Flame* **2010**, *157*, 2333−2339.
(43) Westbrook, C. K.; Pitz, W. J.; Herbinet, O.; Curran, H. J.; Silke, E. J. A Comprehensive Detailed Chemical Kinetic Reaction Mechanism for Combustion of *n*-Alkane Hydrocarbons from *n*-Octane to *n*-Hexadecane. *Combust. Flame* **2009**, *156*, 181−199.
(44) Narayanaswamy, K.; Pepiot, P.; Pitsch, H. A Chemical Mechanism for Low to High Temperature Oxidation of *n*-Dodecane as a Component of Transportation Fuel Surrogates. *Combust. Flame* **2014**, *161*, 866−884.
(45) Zhao, L.; Yang, T.; Kaiser, R. I.; Troy, T. P.; Ahmed, M.; Belisario-Lara, D.; Ribeiro, J. M.; Mebel, A. M. A Combined Experimental and Computational Study on the Unimolecular Decomposition of JP-8 Jet Fuel Surrogates I: *n*-Decane (n-$C_{10}H_{22}$). *J. Phys. Chem. A* **2017**, DOI: 10.1021/acs.jpca.6b11472.
(46) Cool, T. A.; McIlroy, A.; Qi, F.; Westmoreland, P. R.; Poisson, L.; Peterka, D. S.; Ahmed, M. Photoionization Mass Spectrometer for Studies of Flame Chemistry With a Synchrotron Light Source. *Rev. Sci. Instrum.* **2005**, *76*, 094102.
(47) Qi, F.; Yang, R.; Yang, B.; Huang, C. Q.; Wei, L. X.; Wang, J.; Sheng, L. S.; Zhang, Y. W. Isomeric Identification of Polycyclic Aromatic Hydrocarbons Formed in Combustion With Tunable Vacuum Ultraviolet Photoionization. *Rev. Sci. Instrum.* **2006**, *77*, 084101.
(48) Yang, B.; Li, Y. Y.; Wei, L. X.; Huang, C. Q.; Wang, J.; Tian, Z. Y.; Yang, R.; Sheng, L. S.; Zhang, Y. W.; Qi, F. An Experimental Study of the Premixed Benzene/Oxygen/Argon Flame With Tunable Synchrotron Photoionization. *Proc. Combust. Inst.* **2007**, *31*, 555−563.
(49) Yang, B.; Oßwald, P.; Li, Y.; Wang, J.; Wei, L.; Tian, Z.; Qi, F.; Kohse-Höinghaus, K. Identification of Combustion Intermediates in Isomeric Fuel-Rich Premixed Butanol−Oxygen Flames at Low Pressure. *Combust. Flame* **2007**, *148*, 198−209.
(50) Li, Y. Y.; Zhang, L. D.; Tian, Z. Y.; Yuan, T.; Wang, J.; Yang, B.; Qi, F. Experimental Study of a Fuel-Rich Premixed Toluene Flame at Low Pressure. *Energy Fuels* **2009**, *23*, 1473−1485.
(51) Li, Y. Y.; Zhang, L. D.; Tian, Z. Y.; Yuan, T.; Zhang, K. W.; Yang, B.; Qi, F. Investigation of the Rich Premixed Laminar Acetylene/Oxygen/Argon Flame: Comprehensive Flame Structure and Special Concerns of Polyynes. *Proc. Combust. Inst.* **2009**, *32*, 1293−1300.
(52) Li, Y. Y.; Qi, F. Recent Applications of Synchrotron VUV Photoionization Mass Spectrometry: Insight into Combustion Chemistry. *Acc. Chem. Res.* **2010**, *43*, 68−78.
(53) Zhang, L. D.; Cai, J. H.; Zhang, T. C.; Qi, F. Kinetic Modeling Study of Toluene Pyrolysis at Low Pressure. *Combust. Flame* **2010**, *157*, 1686−1697.
(54) Oßwald, P.; Güldenberg, H.; Kohse-Höinghaus, K.; Yang, B.; Yuan, T.; Qi, F. Combustion of Butanol Isomers − A Detailed Molecular Beam Mass Spectrometry Investigation of Their Flame Chemistry. *Combust. Flame* **2011**, *158*, 2−15.
(55) Qi, F. Combustion Chemistry Probed by Synchrotron VUV Photoionization Mass Spectrometry. *Proc. Combust. Inst.* **2013**, *34*, 33−63.
(56) Cool, T. A.; Nakajima, K.; Taatjes, C. A.; McIlroy, A.; Westmoreland, P. R.; Law, M. E.; Morel, A. Studies of a Fuel-Rich Propane Flame With Photoionization Mass Spectrometry. *Proc. Combust. Inst.* **2005**, *30*, 1681−1688.
(57) Cool, T. A.; Wang, J.; Nakajima, K.; Taatjes, C. A.; McIlroy, A. Photoionization Cross Sections for Reaction Intermediates in Hydrocarbon Combustion. *Int. J. Mass Spectrom.* **2005**, *247*, 18−27.
(58) Zhang, F. T.; Kaiser, R. I.; Kislov, V. V.; Mebel, A. M.; Golan, A.; Ahmed, M. A VUV Photoionization Study of the Formation of the Indene Molecule and Its Isomers. *J. Phys. Chem. Lett.* **2011**, *2*, 1731−1735.
(59) Kaiser, R. I.; Belau, L.; Leone, S. R.; Ahmed, M.; Wang, Y. M.; Braams, B. J.; Bowman, J. M. A Combined Experimental and Computational Study on the Ionization Energies of the Cyclic and Linear C_3H Isomers. *ChemPhysChem* **2007**, *8*, 1236−1239.
(60) Kaiser, R. I.; Maksyutenko, P.; Ennis, C.; Zhang, F. T.; Gu, X. B.; Krishtal, S. P.; Mebel, A. M.; Kostko, O.; Ahmed, M. Untangling the Chemical Evolution of Titan's Atmosphere and Surface-from Homogeneous to Heterogeneous Chemistry. *Faraday Discuss.* **2010**, *147*, 429−478.
(61) Kaiser, R. I.; Mebel, A.; Kostko, O.; Ahmed, M. On the Ionization Energies of C_4H_3 Isomers. *Chem. Phys. Lett.* **2010**, *485*, 281−285.
(62) Kaiser, R. I.; Sun, B. J.; Lin, H. M.; Chang, A. H. H.; Mebel, A. M.; Kostko, O.; Ahmed, M. An Experimental and Theoretical Study on the Ionization Energies of Polyynes (H-$(C{\equiv}C)_n$-H;n= 1−9). *Astrophys. J.* **2010**, *719*, 1884−1889.
(63) Kostko, O.; Zhou, J.; Sun, B. J.; Shiuan Lie, J.; Chang, A. H. H.; Kaiser, R. I.; Ahmed, M. Determination of Ionization Energies of C_nN (n= 4−12): Vacuum Ultraviolet Photoionization Experiments and Theoretical Calculations. *Astrophys. J.* **2010**, *717*, 674−682.
(64) Kaiser, R. I.; Krishtal, S. P.; Mebel, A. M.; Kostko, O.; Ahmed, M. An Experimental and Theoretical Study of the Ionization Energies of SiC_2H_x(x= 0, 1, 2) Isomers. *Astrophys. J.* **2012**, *761*, 178−184.
(65) Zhang, F. T.; Kaiser, R. I.; Golan, A.; Ahmed, M.; Hansen, N. A VUV Photoionization Study of the Combustion-Relevant Reaction of the Phenyl Radical (C_6H_5) With Propylene (C_3H_6) in a High

Temperature Chemical Reactor. *J. Phys. Chem. A* **2012**, *116*, 3541−3546.
(66) Golan, A.; Ahmed, M.; Mebel, A. M.; Kaiser, R. I. A VUV Photoionization Study of The Multichannel Reaction of Phenyl Radicals With 1,3-Butadiene Under Combustion Relevant Conditions. *Phys. Chem. Chem. Phys.* **2013**, *15*, 341−347.
(67) Parker, D. S.; Kaiser, R. I.; Troy, T. P.; Ahmed, M. Hydrogen Abstraction/Acetylene Addition Revealed. *Angew. Chem., Int. Ed.* **2014**, *53*, 7740−7744.
(68) Urness, K. N.; Guan, Q.; Golan, A.; Daily, J. W.; Nimlos, M. R.; Stanton, J. F.; Ahmed, M.; Ellison, G. B. Pyrolysis of Furan in a Microreactor. *J. Chem. Phys.* **2013**, *139*, 124305.
(69) Guan, Q.; Urness, K. N.; Ormond, T. K.; David, D. E.; Ellison, G. B.; Daily, J. W. The Properties of a Micro-Reactor for the Study of the Unimolecular Decomposition of Large Molecules. *Int. Rev. Phys. Chem.* **2014**, *33*, 447−487.
(70) *Photoionization Cross Section Database (Version 1.0)*; http://flame.nsrl.ustc.edu.cn/database/. National Synchrotron Radiation Laboratory: Hefei, China, 2011.
(71) Curtiss, L. A.; Raghavachari, K.; Redfern, P. C.; Rassolov, V.; Pople, J. A. Gaussian-3 (G3) Theory for Molecules Containing First and Second-Row Atoms. *J. Chem. Phys.* **1998**, *109*, 7764−7776.
(72) Baboul, A. G.; Curtiss, L. A.; Redfern, P. C.; Raghavachari, K. Gaussian-3 Theory Using Density Functional Geometries and Zero-Point Energies. *J. Chem. Phys.* **1999**, *110*, 7650−7657.
(73) Curtiss, L. A.; Raghavachari, K.; Redfern, P. C.; Baboul, A. G.; Pople, J. A. Gaussian-3 Theory Using Coupled Cluster Energies. *Chem. Phys. Lett.* **1999**, *314*, 101−107.
(74) Frisch, M. J.; Trucks, G. W.; Schlegel, H. B.; Scuseria, G. E.; Robb, M. A.; Cheeseman, J. R.; Scalmani, G.; Barone, V.; Mennucci, B.; Petersson, G. A.; et al. *Gaussian 09, Revision A.1*; Gaussian Inc.: Wallingford CT, 2009.
(75) Werner, H. J.; Knowles, P. J.; Knizia, G.; Manby, F. R.; Schütz, M.; Celani, P.; Györffy, W.; Kats, D.; Korona, T.; Lindh, R.; et al. *MOLPRO*, version 2010.1, a package of ab initio programs, http://www.molpro.net.
(76) Georgievskii, Y.; Miller, J. A.; Burke, M. P.; Klippenstein, S. J. Reformulation and Solution of the Master Equation for Multiple-Well Chemical Reactions. *J. Phys. Chem. A* **2013**, *117*, 12146−12154.
(77) Georgievskii, Y.; Klippenstein, S. J. MESS.2016.3.23, http://tcg.cse.anl.gov/papr/codes/mess.html.
(78) Troe, J. Theory of Thermal Unimolecular Reactions at Low Pressures. I. Solutions of the Master Equation. *J. Chem. Phys.* **1977**, *66*, 4745−4757.
(79) Jasper, A. W.; Oana, C. M.; Miller, J. A. Third-Body" Collision Efficiencies for Combustion Modeling: Hydrocarbons in Atomic and Aiatomic Baths. *Proc. Combust. Inst.* **2015**, *35*, 197−204.
(80) Jasper, A. W.; Miller, J. A. Lennard−Jones Parameters for Combustion and Chemical Kinetics Modeling from Full-Dimensional Intermolecular Potentials. *Combust. Flame* **2014**, *161*, 101−110.
(81) Harding, L. B.; Georgievskii, Y.; Klippenstein, S. J. Predictive Theory for Hydrogen Atom - Hydrocarbon Radical Association Kinetics. *J. Phys. Chem. A* **2005**, *109*, 4646−4656.
(82) Klippenstein, S. J.; Georgievskii, Y.; Harding, L. B. Predictive Theory for the Combination Kinetics of Two Alkyl Radicals. *Phys. Chem. Chem. Phys.* **2006**, *8*, 1133−1147.
(83) *Active Thermochemical Tables*, http://atct.anl.gov/Thermochemical%20Data/version%201.118/index.php.
(84) Sivaramakrishnan, R.; Michael, J. V.; Ruscic, B. High-Temperature Rate Constants for H/D + C_2H_6 and C_3H_8. *Int. J. Chem. Kinet.* **2012**, *44*, 194−205.
(85) Tsang, W. Chemical Kinetic Data-Base for Combustion Chemistry. Part 3. Propane. *J. Phys. Chem. Ref. Data* **1988**, *17*, 887−952.
(86) Baldwin, R. R.; Walker, R. W. Rate Constants for Hydrogen + Oxygen System, and for H Atoms and OH Radicals + Alkanes. *J. Chem. Soc., Faraday Trans. 1* **1979**, *75*, 140−154.
(87) Stewart, J.; Brezinsky, K.; Glassman, I. Supercritical Pyrolysis of Decalin, Tetralin, and *n*-Decane at 700−800K. Product Distribution and Reaction Mechanism. *Combust. Sci. Technol.* **1998**, *136*, 373−390.
(88) Glassman, I.; Yetter, R. A.; Glumac, N. G. *Combustion*; Academic Press: 2014.
(89) Chang, A. H. H.; Mebel, A. M.; Yang, X. M.; Lin, S. H.; Lee, Y. T. Ab Initio/RRKM Approach toward the Understanding of Ethylene Photodissociation. *J. Chem. Phys.* **1998**, *109*, 2748−2761.
(90) Narendrapurapu, B. S.; Simmonett, A. C.; Schaefer, H. F., III; Miller, J. A.; Klippenstein, S. J. Combustion Chemistry: Important Features of the C_3H_5 Potential Energy Surface, Including Allyl Radical, Propargyl + H_2, Allene + H, and Eight Transition States. *J. Phys. Chem. A* **2011**, *115*, 14209−14214.
(91) Hansen, N.; Miller, J. A.; Westmoreland, P. R.; Kasper, T.; Kohse-Höinghaus, K.; Wang, J.; Cool, T. A. Isomer-Specific Combustion Chemistry in Allene and Propyne Flames. *Combust. Flame* **2009**, *156*, 2153−2164.
(92) Miller, J. A.; Senosiain, J. P.; Klippenstein, S. J.; Georgievskii, Y. Reactions over Multiple, Interconnected Potential Wells: Unimolecular and Bimolecular Reactions on a C_3H_5 Potential. *J. Phys. Chem. A* **2008**, *112*, 9429−9438.
(93) Chin, C. H.; Lee, S. H. Comparison of Two-Body and Three-Body Decomposition of Ethanedial, Propanal, Propenal, *n*-Butane, 1-Butene, and 1,3-Butadiene. *J. Chem. Phys.* **2012**, *136*, 024308.
(94) Ribeiro, J. M.; Mebel, A. M. Reaction Mechanism and Product Branching Ratios of the CH + C_3H_6 Reaction: A Theoretical Study. *J. Phys. Chem. A* **2016**, *120*, 1800−1812.
(95) Backx, C.; Wight, G. R.; Wiel, M. J. V. d. Oscillator Strengths (10−70 eV) for Absorption, Ionization and Dissociation in H_2, HD and D_2, Obtained by an Electron-Ion Coincidence Method. *J. Phys. B: At. Mol. Phys.* **1976**, *9*, 315.
(96) Savee, J. D.; Soorkia, S.; Welz, O.; Selby, T. M.; Taatjes, C. A.; Osborn, D. L. Absolute Photoionization Cross-Section of the Propargyl Radical. *J. Chem. Phys.* **2012**, *136*, 134307.
(97) Samson, J. A. R.; Haddad, G. N.; Masuoka, T.; Pareek, P. N.; Kilcoyne, D. A. L. Ionization Yields, Total Absorption, and Dissociative Photoionization Cross-Sections of CH_4 from 110−950-A. *J. Chem. Phys.* **1989**, *90*, 6925−6932.
(98) Gans, B.; Garcia, G. A.; Boyé-Péronne, S.; Loison, J.-C.; Douin, S.; Gaie-Levrel, F.; Gauyacq, D. Absolute Photoionization Cross Section of the Ethyl Radical in the Range 8−11.5 eV: Synchrotron and Vacuum Ultraviolet Laser Measurements. *J. Phys. Chem. A* **2011**, *115*, 5387−5396.
(99) Yang, B.; Wang, J.; Cool, T. A.; Hansen, N.; Skeen, S.; Osborn, D. L. Absolute Photoionization Cross-Sections of Some Combustion Intermediates. *Int. J. Mass Spectrom.* **2012**, *309*, 118−128.
(100) Robinson, J. C.; Sveum, N. E.; Neumark, D. M. Determination of Absolute Photoionization Cross Sections for Isomers of C_3H_5: Allyl and 2-Propenyl Radicals. *Chem. Phys. Lett.* **2004**, *383*, 601−605.
(101) Koizumi, H. Predominant Decay Channel for Superexcited Organic-Molecules. *J. Chem. Phys.* **1991**, *95*, 5846−5852.
(102) Wang, J.; Yang, B.; Cool, T. A.; Hansen, N.; Kasper, T. Near-Threshold Absolute Photoionization Cross-Sections of Some Reaction Intermediates in Combustion. *Int. J. Mass Spectrom.* **2008**, *269*, 210−220.
(103) Zhou, Z. Y.; Zhang, L. D.; Xie, M. F.; Wang, Z. D.; Chen, D. N.; Qi, F. Determination of Absolute Photoionization Cross-Sections of Alkanes and Cyclo-Alkanes. *Rapid Commun. Mass Spectrom.* **2010**, *24*, 1335−1342.

NOTE ADDED AFTER ASAP PUBLICATION

This paper was published ASAP on February 1, 2017 with production errors. The corrected paper was reposted on February 6, 2017.

DOI: 10.1021/acs.jpca.6b11817
J. Phys. Chem. A 2017, 121, 1281−1297